LETTERS
https://doi.org/10.1038/s42255-021-00479-4
nature metabolism

Check for updates

Pharmacological inhibition of fatty acid synthesis blocks SARS-CoV-2 replication

Junjun Chu[1,7], Changsheng Xing[1,7], Yang Du[1,7], Tianhao Duan[1], Siyao Liu[2], Pengfei Zhang[2], Chumeng Cheng[3], Jill Henley[4], Xin Liu[1], Chen Qian[1], Bingnan Yin[1], Helen Yicheng Wang[1,5] and Rong-Fu Wang[1,5,6] ✉

Caused by severe acute respiratory syndrome coronavirus 2 (SARS-CoV-2), COVID-19 is a virus-induced inflammatory disease of the airways and lungs that leads to severe multi-organ damage and death. Here we show that cellular lipid synthesis is required for SARS-CoV-2 replication and offers an opportunity for pharmacological intervention. Screening a short-hairpin RNA sublibrary that targets metabolic genes, we identified genes that either inhibit or promote SARS-CoV-2 viral infection, including two key candidate genes, *ACACA* and *FASN*, which operate in the same lipid synthesis pathway. We further screened and identified several potent inhibitors of fatty acid synthase (encoded by *FASN*), including the US Food and Drug Administration-approved anti-obesity drug orlistat, and found that it inhibits in vitro replication of SARS-CoV-2 variants, including more contagious new variants, such as Delta. In a mouse model of SARS-CoV-2 infection (K18-hACE2 transgenic mice), injections of orlistat resulted in lower SARS-CoV-2 viral levels in the lung, reduced lung pathology and increased mouse survival. Our findings identify fatty acid synthase inhibitors as drug candidates for the prevention and treatment of COVID-19 by inhibiting SARS-CoV-2 replication. Clinical trials are needed to evaluate the efficacy of repurposing fatty acid synthase inhibitors for severe COVID-19 in humans.

The coronavirus disease 2019 (COVID-19) pandemic is the third zoonotic coronavirus (CoV) outbreak in the last 20 years, following severe acute respiratory syndrome (SARS) in 2003 and Middle East respiratory syndrome in 2012, both of which were associated with severe clinical symptoms and high mortality rates[1–3]. SARS-CoV-2 infection and disease severity have been linked to pre-existing disease conditions such as obesity[4–7], in addition to age and sex[8]. Despite great efforts to identify therapeutics for the effective treatment of patients with COVID-19, particularly those with obesity and other pre-existing conditions, treatment options remain limited. Many studies have targeted SARS-CoV-2 virus main protease (M^{pro}) as a major target for drug screening to identify new drugs for COVID-19 treatment[9–12]. To accelerate development of therapeutic drugs for COVID-19 treatment, other studies have performed high-throughput screening of clinical-stage or US Food and Drug Administration (FDA)-approved small molecules to repurpose known drugs[13–15]. This approach has led to the identification of remdesivir, a viral RNA polymerase inhibitor and its approval as emergency use authorization for the treatment of patients with COVID-19 (refs. [16,17]). However, the clinical efficacy of remdesivir is limited based on clinical trial data, particularly for patients with severe COVID-19 (refs. [17,18]).

Besides drugs targeting the viral proteins for their ability to inhibit viral infection and replication, recent studies have shown that host proteins are critically required for SARS-CoV-2 infection and replication[19–24]. A recent study showed that the drug plitidepsin (Aplidin), which targets the host protein eEF1A, exhibits potent anti-SARS-CoV-2 activity in cell cultures and mouse models[25]. Another US FDA-approved inhibitor topotecan (TPT) targeting topoisomerase 1 has been reported to suppress the lethal inflammation induced by SARS-CoV-2 and reduce morbidity and mortality in a preclinical mouse model[26]. Thus, identification of additional host biological pathways and corresponding drugs is urgently needed to facilitate new drug development for the treatment of the COVID-19 disease and prevent viral spread.

Although it is largely unknown why individuals with obesity are closely linked to the high risk of SARS-CoV-2 infection and severe disease, metabolic pathways (particularly the lipid metabolism) have been implicated in viral entry into the cells through viral protein palmitoylation and membrane fusion[27–29]. The SARS-CoV-2 virus can hijack the host cell metabolism by remodeling the host folate (one-carbon metabolism) and tricarboxylic acid (TCA) cycle metabolism to acquire the building blocks required for replication[30,31]. Understanding how SARS-CoV-2 alters the host cell metabolism may lead to identification of potential new therapeutic targets for COVID-19. Targeting metabolic pathways may particularly be a potential antiviral strategy for COVID-19 treatment[29]. In efforts to identify new host pathways and proteins that are critically required for SARS-CoV-2 infection, we screened a sublibrary of short hairpin (sh)RNAs targeting 95 metabolic genes in HEK293T-hACE2 (stably expressing human ACE2) to test for their ability to inhibit infectious-clone-derived mNeonGreenSARS-CoV-2 reporter virus (SARS-CoV-2-mNG) infection[32]. Each gene was targeted with an average of three shRNAs. HEK293T-hACE2 cells were transfected with shRNAs, followed by infection with SARS-CoV-2-mNG viruses[32]. SARS-CoV-2 infection efficiency was determined based on green fluorescence intensity (Fig. 1a). After two rounds of independent screenings, we analyzed the data in a correlation plot for

[1]Department of Medicine, Keck School of Medicine, University of Southern California, Los Angeles, CA, USA. [2]Department of Molecular Microbiology and Immunology, Keck School of Medicine, University of Southern California, Los Angeles, CA, USA. [3]Mork Family Department of Chemical Engineering and Materials Science, University of Southern California, Los Angeles, CA, USA. [4]The Hastings and Wright Laboratories, Keck School of Medicine, University of Southern California, Los Angeles, CA, USA. [5]Department of Pediatrics, Children's Hospital Los Angeles, Keck School of Medicine, University of Southern California, Los Angeles, CA, USA. [6]Norris Comprehensive Cancer Center, Keck School of Medicine, University of Southern California, Los Angeles, CA, USA. [7]These authors contributed equally: Junjun Chu, Changsheng Xing, Yang Du. ✉e-mail: rongfuwa@usc.edu

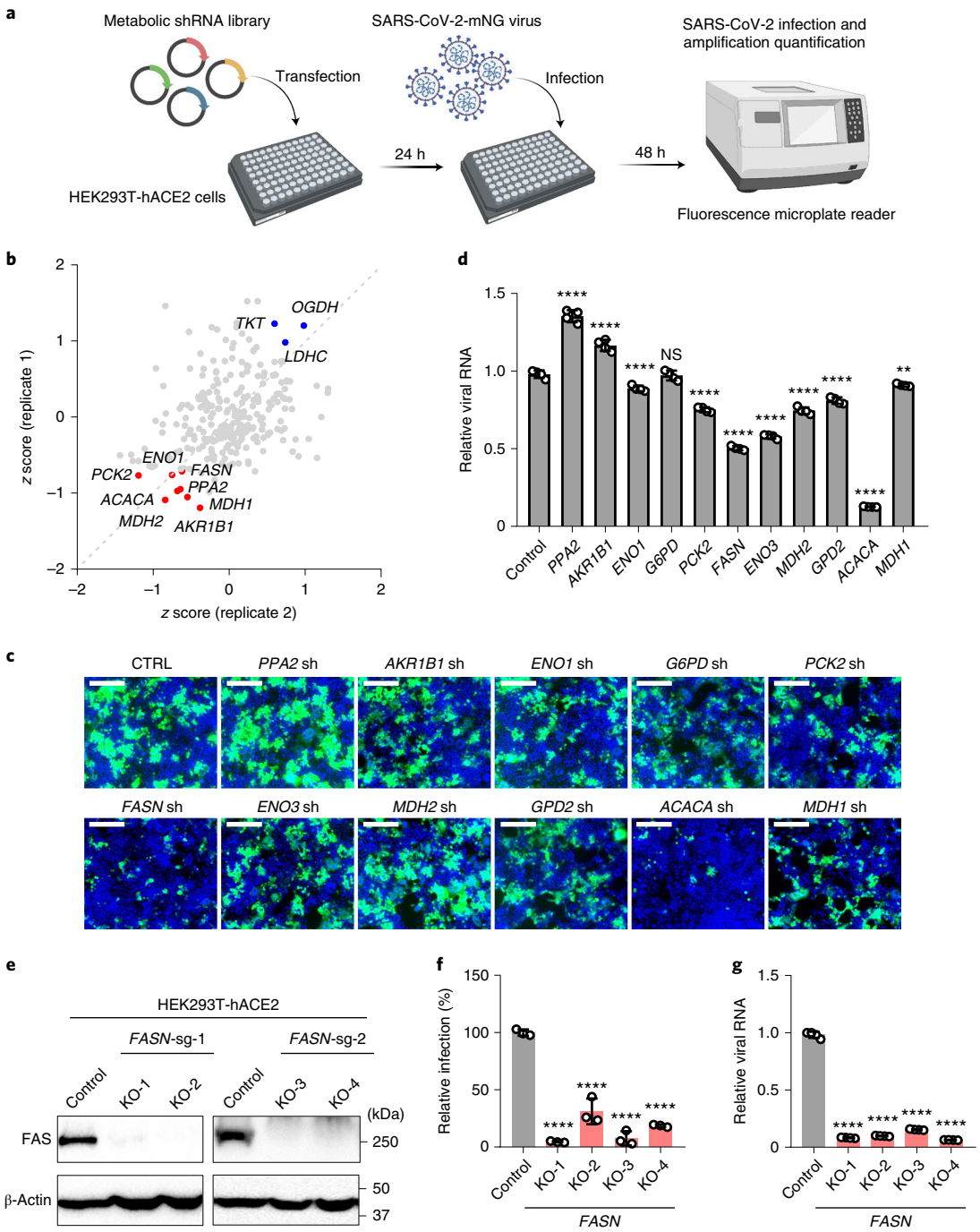

Fig. 1 | ShRNA library screen identifies *FASN* as a critical factor for SARS-CoV-2 infection. a, A schematic diagram of shRNA sublibrary screening against SARS-CoV-2 infection (created with BioRender.com). **b**, Correlation plot indicates activity (*z* score) of each gene in the two replicate screens. **c**,**d**, Validation of gene hits. HEK293T-hACE2 cells were transfected with indicated shRNAs. After 3 d, cells were infected SARS-CoV-2-mNG at an MOI of 0.01. Cells were subjected to fluorescence microscopy analyses (**c**) and qPCR analysis (**d**) at 24 h post infection (hpi). Scale bar, 200 μm. **e**, Generation of *FASN* KO HEK293T-hACE2 cells. Representative images of western blot analysis for FAS expression in HEK293T-hACE2 cells transduced with puro-guide control, *FASN* sgRNA1 (clone KO-1 and KO-2) or *FASN* sgRNA2 (clone KO-3 and KO-4) lentivirus. **f**, *FASN* KO inhibits SARS-CoV-2 infection. Control and *FASN* KO HEK293T-hACE2 cells were infected with SARS-CoV-2-mNG at an MOI of 0.01. The cells were imaged with fluorescence microscopy at 24 hpi. Viral infection was quantified by green fluorescence intensity and normalized by nuclear dye Hoechst 33342. **g**, *FASN* KO inhibits SARS-CoV-2 viral replication. Control and *FASN* KO HEK293T-hACE2 cells were infected with SARS-CoV-2 (USA-WA1/2020 strain unless otherwise stated) with an MOI of 0.01. Cells were subjected to qPCR analysis for viral RNA at 24 hpi. Data in **d**,**f**,**g** are representative of three independent experiments and are plotted as mean ± s.d. ($n = 3$ (**f**), $n = 4$ (**d**,**g**) per group). Experiments in **c**,**e** were independently repeated three times with similar results. Statistical analyses were performed with one-way analysis of variance (ANOVA) followed by Dunnett's post-test compared with control cells (**d**,**f**,**g**). $^{**}P < 0.01$, $^{****}P < 0.0001$; NS, not significant.

consistency (z score) and found that the knockdown of several key genes (labeled in red) conferred the host cells' resistance to SARS-CoV-2 infection (Fig. 1b and Supplementary Table 1). Similar results were obtained with knockdown of selected genes with specific shRNAs in HEK293T-hACE2 cells infected with SARS-CoV-2-mNG viruses (Fig. 1c,d). Among them, the knockdown of *FASN* and *ACACA*, which are key rate-limiting enzymes in fatty acid synthesis, markedly reduced SARS-CoV-2 infection. *ACACA* encodes acetyl-CoA carboxylase-α (ACC1), a rate-limiting enzyme that converts acetyl-CoA to malonyl-CoA. *FASN* encodes fatty acid synthase (FAS), a whole enzyme of FAS containing two identical multifunctional proteins. FAS synthesizes palmitate from acetyl-CoA to malonyl-CoA in the presence of NADPH. Therefore, both ACC1 and FAS act in concert to synthesize palmitate (Extended Data Fig. 1a), a key product of subsequent lipid synthesis.

To further substantiate the role of FAS in response to SARS-CoV-2 infection, we generated *FASN* knockout (KO) HEK293T-hACE2 cells (Fig. 1e). We showed that FAS-deficient cells markedly repressed the infection of the SARS-CoV-2-mNG virus (Fig. 1f) and the amount of viral RNA in the infected cells (Fig. 1g). Furthermore, we validated our observation in Caco-2 cells and showed that the KO of *FASN* significantly decreased the amount of SARS-CoV-2 viral RNA and infectious viral particles in the supernatant (Extended Data Fig. 1b–d). Taken together, these results suggest that *FASN* deficiency markedly inhibits SARS-CoV-2 infection.

As many FAS inhibitors are available, we next explore the therapeutic potential of FAS as a target for the treatment of COVID-19. To this end, we screened 22 FAS inhibitors for their ability to inhibit SARS-CoV-2 infection. HEK293T-hACE2 cells were pre-treated with dimethylsulfoxide (DMSO) control or FAS inhibitors for 16 h and then infected with the SARS-CoV-2-mNG virus. Among the 22 inhibitors tested at a final concentration of 5 μM, we found 11 FAS inhibitors that could markedly inhibit SARS-CoV-2 infection without obvious toxicity (Fig. 2a). Among them, orlistat is a US FDA-approved anti-obesity drug, while TVB-2640 is under phase II clinical trials as an anticancer therapy. Orlistat and TVB-2640 inhibit lipases to reduce the absorption of dietary fat and FAS to reduce lipid synthesis[33]. Next, we performed dose titration of seven inhibitors with the most promising inhibitory activity. Remdesivir was used as a positive control in our assay. TVB-3664 strongly inhibited SARS-CoV-2 with a half maximal effective concentration (EC_{50}) value of 0.07 nM, which was five times more potent than remdesivir (EC_{50} = 0.4 nM) (Fig. 2b). Orlistat and TVB-2640 also markedly inhibited SARS-CoV-2 with EC_{50s} of 390 nM and 4 nM, respectively. Similarly, the remaining FAS inhibitors TVB-3166, GSK-214069, FASN-IN-4 and FT113 inhibited SARS-CoV-2 with an EC_{50} of 11 nM, 0.9 nM, 18.6 nM and 17 nM, respectively (Fig. 2b). Furthermore, the cytotoxicity of these seven inhibitors was evaluated by 3-(4,5-dimethylthiazol-2-yl)-2,5-diphenyltetrazolium bromide (MTT) assay in parallel with their antiviral activity. We did not observe significant toxicity at the working concentration of all seven inhibitors (Fig. 2b). Notably, the FAS inhibitor TVB-3664 (20 nM) still had a strong inhibitory effect even when the initial viral amount was increased by 100 times (multiplicity of infection (MOI) from 0.01 to 1). By contrast, remdesivir (20 nM) failed to inhibit SARS-CoV-2 infection at this level (Fig. 2c and Extended Data Fig. 2a).

We further tested the ability of FAS inhibitors to control viral replication. After the pre-treatment of selected inhibitors and the infection of SARS-CoV-2, the infectious viral particles in the supernatant and viral RNA in infected cells were quantified by qPCR and plaque assay, respectively. Consistent with SARS-CoV-2-mNG screening, TVB-3664, TVB-2640 and orlistat markedly inhibited the infectivity and replication of the SARS-CoV-2 virus (USA-WA1/2020 strain) (Fig. 2d,e). The replication of the SARS-CoV-2 virus was significantly reduced in all FAS inhibitor-treated HEK293T-hACE2 cells at the levels of viral RNA and infectious viral titers (Extended Data Fig. 2b,c). To further test the antiviral activity of the FAS inhibitors in other cell types, we treated human lung cell lines (NCI-H1355 and NCI-H1437), a human colon cell line (Caco-2) and mouse embryonic fibroblasts stably expressing hACE2 (MEF-hACE2) with the selected FAS inhibitors and found that these FAS inhibitors markedly inhibited SARS-CoV-2 in all the cells we tested, as indicated by virally infected green fluorescence-positive cells, viral RNA levels and infectious viral titers (Extended Data Fig. 2d–f).

To determine the antiviral activity of these FAS inhibitors after SARS-CoV-2 infection, we performed time-course experiments. TVB-3664, TVB-2640 and orlistat were added to HEK293T-hACE2 cells at different time points (−16, −1, 0, +1, +2, +4 and +6 h with infection time set as h 0). We found that all three inhibitors could potently inhibit SARS-CoV-2 even at 4–6 h post-infection (Fig. 2f). Taken together, our results suggest that FAS inhibitors can potently inhibit SARS-CoV-2 infection and replication in several tested cell lines.

A previous study shows that the palmitoylation modification of the SARS-CoV-2 spike protein is essential for viral infectivity[34]. FAS inhibitors reduced cellular levels of free fatty acids and palmitoylated proteins (Extended Data Fig. 3a,b). Furthermore, addition of BSA-conjugated palmitic acid (PA-BSA) reversed the antiviral effects of FASN KO and FAS inhibitors in a dose-dependent manner (Extended Data Fig. 3c,d). However, palmitic acid only partially reversed the antiviral effects of orlistat, probably because orlistat can also inhibit lipases in addition to its inhibitory activity on FAS.

Orlistat has been approved to treat obesity. Because of its clinical safety profile, we next tested whether orlistat has in vivo anti-SARS-CoV-2 activity. The K18-hACE2 mouse model has been

Fig. 2 | Screening of FAS inhibitors for anti-SARS-CoV-2 activity. a, In vitro screening of FAS inhibitors. HEK293T-hACE2 cells were pre-treated with 22 fatty acid metabolism-related inhibitors (at a final concentration of 5 μM) from 16 h before and during the infection. Inhibitor-treated cells were infected with the SARS-CoV-2-mNG virus at an MOI of 0.01. The cells were imaged with fluorescence microscopy at 24 hpi. Viral infection was quantified by green fluorescence intensity and normalized by nuclear dye Hoechst 33342. † ACSS2 is toxic and the treated cell died after treatment. **b**, Dose titration of selected inhibitors for anti-SARS-CoV-2 activity. Various concentrations of the selected inhibitors were used to assess their ability to inhibit SARS-CoV-2-mNG infection. Relative infection (black curve), cell viability (red curve) and EC_{50} value of antiviral ability are indicated. **c**, Direct comparison of FAS inhibitors with remdesivir by challenging with increased amounts of virus. HEK293T-hACE2 cells were treated with TVB-3664 (20 nM) and remdesivir (20 nM) and infected with SARS-CoV-2-mNG virus at MOI = 0.01, 0.1 or 1. Relative infection was quantified by the green fluorescence intensity at 16 hpi. **d**,**e**, Anti-SARS-CoV-2 ability of FAS inhibitors in HEK293T-hACE2 cells. Viral RNA (in the infected cells) and infectious viral particles (in the supernatant) were detected by qPCR (**d**) and plaque assay (**e**), respectively (orlistat 1 μM, TVB-2640 100 nM and TVB-3664 20 nM). **f**, Time-of-addition assay for the antiviral ability of FAS inhibitors in HEK293T-hACE2 cells. FAS inhibitors were added at different time points before and after SARS-CoV-2 infection. Viral RNA was detected at 24 hpi by qPCR. Ctrl, control. Data in **a**,**c**–**f** are representative of three independent experiments and are plotted as the mean ± s.d. (n = 3 (**a**–**c**), n = 4 (**d**–**f**) per group). Data in **b** are plotted as the mean ± s.d. for relative infection (quantitative fluorescence) and relative cell viability (MTT) performed in biological triplicate. EC_{50} value was calculated by a four-parameter logistic nonlinear regression model. Statistical analyses were performed using one-way ANOVA followed by Dunnett's post-test (**a**,**d**–**f**) or two-way ANOVA followed by Tukey post-test (**c**). $^{*}P < 0.05$, $^{****}P < 0.0001$ versus DMSO-treated cells (**a**,**d**–**f**) or remdesivir-treated cells (**c**). NS, not significant.

successfully used for SARS-CoV-2 infection and COVID-19 diseases[35,36]. We infected hACE2 transgenic mice with SARS-CoV-2 virus (intranasal infection, 1×10^4 plaque-forming units (p.f.u.) per mouse), followed by intraperitoneal injection of orlistat (8 mg kg^{-1}) daily starting at day 0 (Fig. 3a). DMSO/PBS buffer served as a control treatment. We found that SARS-CoV-2-infected mice treated with DMSO/PBS manifested a 15% loss of body weight and died between days 5–8 (Fig. 3b,c). In contrast, the orlistat treatment of SARS-CoV-2-infected mice markedly prolonged their survival, with 50% of the orlistat-treated SARS-CoV-2-infected mice gradually recovering their body weight and surviving (Fig. 3b,c). TVB-2640 also showed significant in vivo antiviral activity and protected

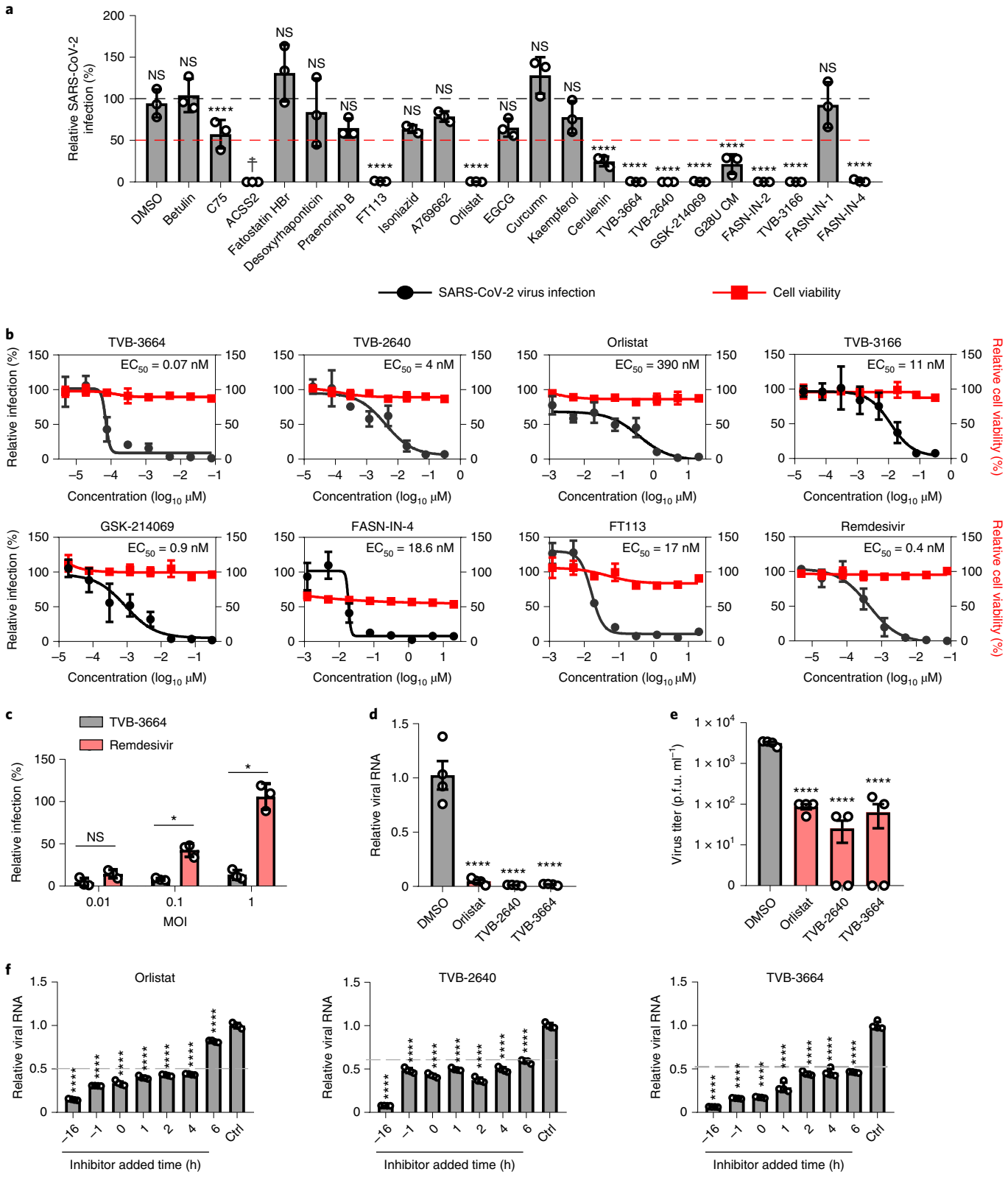

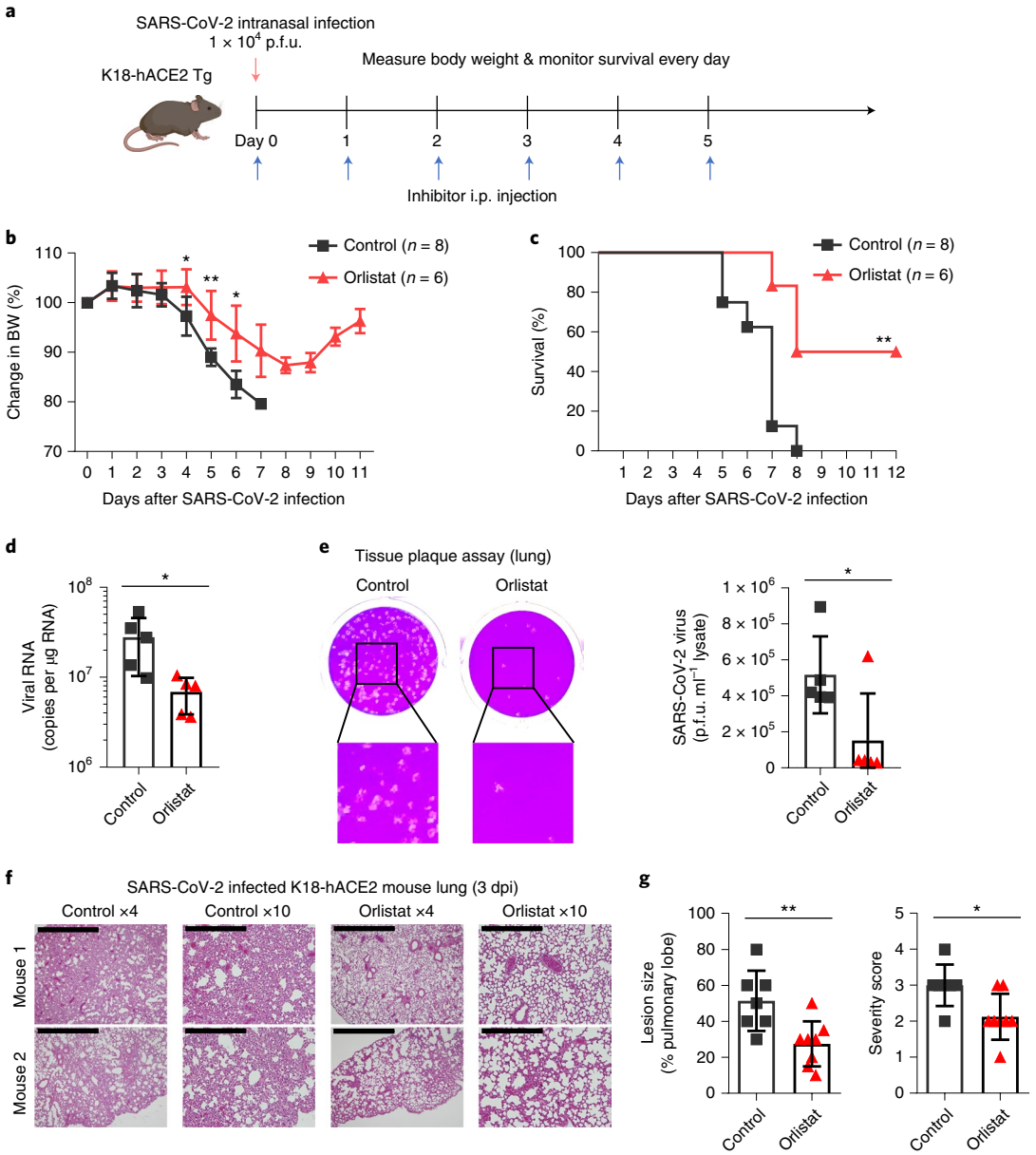

Fig. 3 | FAS inhibitors show in vivo anti-SARS-CoV-2 infection and prolong the infected mouse survival. a, A schematic presentation of the experiment design for SARS-CoV-2 infection in the hACE2 transgenic mouse model (created with BioRender.com). **b**,**c**, Orlistat reduces body weight loss and prolongs the mouse survival after SARS-CoV-2 infection. K18-hACE2 transgenic mice were infected with SARS-CoV-2 virus (intranasal infection, 1×10^4 p.f.u. per mouse, USA-WA1/2020) and intraperitoneally (i.p.) injected with orlistat (8 mg kg^{-1} body weight) ($n=6$) or DMSO/PBS control buffer ($n=8$) daily from day 0 to day 5. Body weight changes (**b**) and survival curves (**c**) were observed and analyzed. **d**–**g**, Orlistat reduces viral replication and disease progression in lung tissues after SARS-CoV-2 infection. K18-hACE2 transgenic mice were infected with SARS-CoV-2 and i.p. injection with orlistat. **d**, Local viral production by qPCR analysis with lung tissue RNA samples on day 3 ($n=5$ for each group). **e**, Viral titration by plaque assay with the supernatant of homogenized lung tissues on day 3 ($n=5$ for each group). **f**, Histopathology of formalin-fixed and hematoxylin and eosin (H&E)-stained lung tissues on day 3 ($n=7$ for control group and $n=8$ for orlistat group). dpi, days post infection. **g**, Analyses of pulmonary lesion sizes and pathological severity scores, based on the percentage of affected area in lung tissues. Representative images of plaque assay (**e**) and immunohistochemistry (IHC) staining (**f**) were presented. Scale bar, 400 μm for ×10 and 1 mm for ×4. **b** and **c** show combined data of two independent experiments and are plotted as the mean ± s.d., **d**–**g** are representative data of two independent experiments and are plotted as the mean ± s.d. Statistical analyses were performed using two-way ANOVA followed by Sidak's post-test (**b**), two-side unpaired Student's *t*-test (**d**,**e**,**g**) and Mantel–Cox log-rank test (**c**). $^*P<0.05$; $^{**}P<0.01$.

SARS-CoV-2-infected mice for survival (Extended Data Fig. 4a,b). Furthermore, the capacity of orlistat to control local SARS-CoV-2 replication was evaluated in lung tissues from infected hACE2 transgenic mice. We found that orlistat treatment inhibited SARS-CoV-2 replication in lung tissues, with significantly decreased viral RNA amounts (Fig. 3d) and infectious viral titers (Fig. 3e). Consistently, histopathology analysis also revealed a reduction in lung inflammation in orlistat-treated mice compared with vehicle-treated mice (Fig. 3f,g and Extended Data Fig. 4c,d). Similar results were obtained using a different animal model, in which wild-type (WT) C57BL/6J (B6) mice were intranasally infected with adenovirus (Adv)-hACE2 to induce ACE2 expression in lung epithelial cells[36].

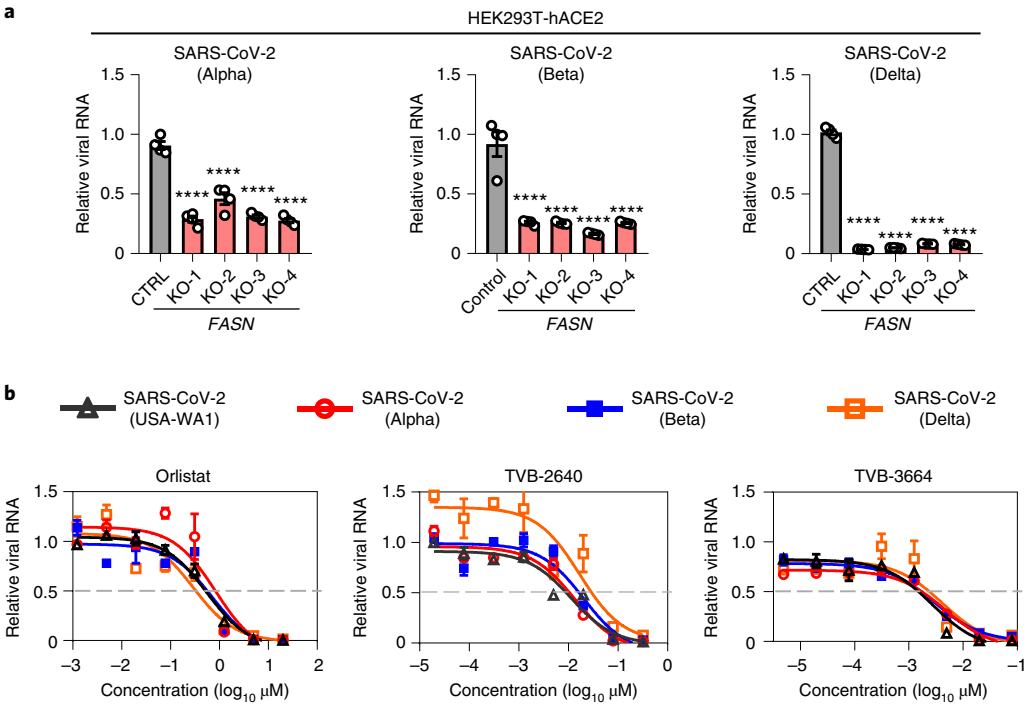

Fig. 4 | FAS inhibitors show antiviral activity against SARS-CoV-2 new variants. a, FAS deficiency inhibits SARS-CoV-2 new variants. Control and *FASN* KO HEK293T-hACE2 cells were infected with α, β and δ strains with an MOI of 0.01. The cells were subjected to qPCR analysis for viral RNA at 24 hpi. **b**, Antiviral ability evaluation of FAS inhibitors against SARS-CoV-2 variants (B.1.1.7 and B.1.351). HEK293T-hACE2 cells were treated with orlistat, TVB-2640 and TVB-3664 at the indicated concentrations and infected with SARS-CoV-2 or variants with an MOI of 0.01. Relative viral RNA was detected by qPCR at 24 hpi. Data in **a**,**b** are representative of three independent experiments and are plotted as the mean ± s.d. ($n = 4$ (**a**,**b**) per group). Data in **b** were normalized to the average of DMSO-treated cells. Statistical analysis in **a** was performed using one-way ANOVA followed by Dunnett's post-test, all experimental groups compared with scramble sgRNA-transduced HEK293T-hACE2 cells. ****$P < 0.0001$.

We showed that the administration of orlistat could significantly inhibited the disease's progression with decreased histopathology in the lungs (Extended Data Fig. 4f,g), which is consistent with the observations in K18-hACE2 mice. To determine whether orlistat treatment has therapeutic effects on the disease's progression after viral infection, we treated SARS-CoV-2-infected mice at day zero or day one after infection and found that orlistat treatment on day one after infection could also significantly prolong the animal survival compared with the control group, but failed to rescue infected mice (Extended Data Fig. 4e), suggesting that orlistat treatment has therapeutic effects even after SAR-CoV-2 infection. Taken together, these results suggest that orlistat treatment exhibits strong in vivo anti-SARS-CoV-2 activity, inhibits lung inflammation and disease progression and protects host survival after infection, thus providing a promising clinical candidate for the treatment of COVID-19.

New SARS-CoV-2 variants α (lineage B.1.1.7), β (lineage B.1.351) and δ (lineage B.1.617.2), which were initially detected in the United Kingdom, South Africa and India, respectively, are rapidly spreading globally, raising major public health concerns. While the Alpha variant is associated with increased transmissibility[37] and risk of death compared with other variants[38,39], the Beta variant may also increase the risk of infection in immunized individuals by escaping from vaccine-induced antibody neutralization[40,41]. Recently, the Delta variant has become a predominant SARS-CoV-2 variant that accounts for over 90% of the new cases in the United States, thus raising major concerns about this surge and reducing protection through neutralizing antibodies in vaccinated individuals[42,43]. Consequently, identification of innovative drugs to inhibit new SARS-CoV-2 variants is urgently needed. To this end, we tested whether FAS inhibitors could inhibit the infection and replication of the new SARS-CoV-2 variants. We infected HEK293T-hACE2 cells with SARS-CoV-2 variants and found that FAS deficiency markedly reduced viral RNA levels in *FASN* KO cells, compared with control cells (Fig. 4a). Notably, FAS inhibitors (TVB-3664, TVB-2640 and orlistat) could strikingly inhibit SARS-CoV-2 new variants with similar inhibitory effects on the early-lineage SARS-CoV-2 (USA-WA1/2020) virus (Fig. 4b). Similar inhibitory activities of these FAS inhibitors were observed in NCI-H1355 and MEF-hACE2 cells infected with SAR-CoV-2 variants (Extended Data Fig. 5a,b). Taken together, our data suggest that FAS inhibitors effectively inhibit SARS-CoV-2 and its dominant variants, suggesting broad antiviral activity against early-lineage SARS-CoV-2 and new variants.

The findings presented here provide direct evidence that the ACC1-FAS lipid synthesis pathway is critically required for SARS-CoV-2 infection and replication. Notably, we identified several FAS inhibitors, including the US FDA-approved drug orlistat that markedly reduce SARS-CoV-2 infection and disease progression in cell cultures and mouse models. During our work, several groups have shown that host proteins and factors are critically required for SARS-CoV-2 infection and replication[19–24]. Although a lipid metabolism, particularly cholesterol, has been demonstrated to play a role in SARS-CoV-2 infection, ACC1 and FAS in the lipid synthesis pathway have not been reported, especially for inhibiting the new variants.

Individuals with pre-existing conditions such as obesity have been closely associated with a high risk of SARS-CoV-2 infection, severe COVID-19 disease progression and even death, but the underlying mechanisms remain largely unknown. The infection and replication of the coronavirus involve multiple critical interac-

tions with host cell membranes, including during viral entry and virus release[44]. Lipids represent the structural foundations of cellular and viral membranes, thus are important for viral replication by regulating the membrane fusion, envelopment and transformation[44]. Therefore, inhibition of the lipid synthesis pathways may lead to reduced viral infection[44]. FAS is one of the major targets for obesity and also a candidate target for anticancer therapy. The first FAS inhibitor, orlistat, is an orally bioavailable nonprescription drug for obesity management that is reasonably priced and generally well tolerated by healthy people[45]. It should be noted that the early treatment of orlistat as a preventive medicine for obesity and SARS-CoV-2 infection could be the key to inhibit viral replication, whereas the late treatment, after the onset of symptoms or severe disease, might be less efficacious. Although a previous study reports the antiviral potential of orlistat in multiple viruses, such as dengue virus, Japanese encephalitis virus, Zika virus and chikungunya virus[46], but none of them has reached clinical treatment for viral pathogens. A recent work also shows that orlistat can suppress SARS-CoV-2 replication in an in vitro study[47]. TVB-2640 is the second clinical level FAS inhibitor and is now under phase II clinical study for cancer treatment. Both orlistat and TVB-2640 have established safety profiles. As TVB-2640 is ~100 times lower than orlistat in HEK293T-hACE2 cells, further studies on TVB-2640 as a promising therapeutic candidate are warranted. Taken together, our study has identified orlistat and TVB-2640 as potential anti-SARS-CoV-2 drugs with in vivo efficacy, therefore raising the possibility for further testing these drugs in other SARS-CoV-2 animal models and future human clinical studies to test their protective and therapeutic effects on infection of SARS-CoV-2 and its emerging variants.

Methods

Cells and viruses. HEK293T-hACE2 (BEI Resources, cat. no. NR-52511), Vero-E6 (ATCC, cat. no. CRL-1586), MEF-hACE2 (mouse embryonic fibroblasts transduced with human ACE2 were generated in our laboratory) were cultured in Dulbecco's modified Eagle medium (DMEM; Thermo Fisher) supplemented with 10% FBS. Caco-2 (ATCC, cat. no. HTB-37) cells were cultured in Eagle's minimum essential medium (Thermo Fisher) supplemented with 20% FBS. NCI-H1355 (ATCC, cat. no. CRL-5865) and NCI-H1437 (ATCC, cat. no. CRL-5872) cells were cultured in RPMI 1640 medium (Thermo Fisher) supplemented with 10% FBS. All these cell lines were supplemented with penicillin (100 U ml^{-1}, Thermo Fisher) and streptomycin (100 µg ml^{-1}, Thermo Fisher) and maintained at 37 °C in a humidified atmosphere with 5% CO_2. In this manuscript, the SARS-CoV-2 virus specifically refers to the USA-WA1/2020 strain unless otherwise stated, which was originally isolated from an oropharyngeal swab from a patient with a respiratory illness who developed clinical disease (COVID-19) in January 2020 in Washington, USA. SARS-CoV-2 virus (USA-WA1/2020) was obtained from University of Southern California (USC) BSL3 Core and the original virus was requested from BEI Resources (NR-52281). SARS-CoV-2-mNG virus (icSARS-CoV-2-mNG) was a generous gift from P.-Y. Shi's laboratory at the University of Texas Medical Branch. SARS-CoV-2 Alpha variant (lineage B.1.1.7), Beta variant (lineage B.1.351) and Delta variant (lineage B.1.617.2) strains were obtained from USC BSL3 (biosafety level 3) Core and the original viruses were obtained from BEI Resources (NR-54000, NR-54009 and NR-55611). Viral stocks used in this study were sequence verified by USC BSL3 Core. All SARS-CoV-2 virus-related BSL3 experiments were conducted in the Hastings Foundation and The Wright Foundation laboratories at USC. The standard operating procedure of the BSL3 level experiments has been validated and approved. Biological use authorization was approved by the biosafety committee of USC.

Animals and in vivo procedures. K18-hACE2 transgenic mice were purchased from Jackson Laboratory (cat. no. 034860), then bred and maintained in specific-pathogen-free facilities at the USC. Genotyping was performed with primers from Jackson Laboratory and hemizygous mice were used in our study. C57BL/6J mice were purchased from Jackson Laboratory (cat. no. 000664). In all experiments, mice were treated from 8–10 weeks old; and both males and females were used. Mice were housed under a 12:12 light:dark cycle and all the facilities are accredited by the Association for Assessment and Accreditation of Laboratory Animal Care International. All animal studies were approved by the Institutional Animal Care and Use Committee of the USC.

For in vivo SARS-CoV-2 infection, K18-hACE2 transgenic mice were first transferred into the ABSL3 facility of USC. All animal procedures (including infection, injection, weighing and killing) were performed after anesthesia by isoflurane. Mice were intranasally infected with 10^4 p.f.u. of SARS-CoV-2 virus (USA-WA1/2020) in 30 µl serum-free DMEM. Orlistat was first dissolved in DMSO and diluted in PBS for intraperitoneal injection. The same volume of DMSO/PBS buffer was used in control groups. Orlistat or TVB-2640 was intraperitoneally injected daily (8 mg kg^{-1} body weight) from the indicated starting time points to day 5 post-infection.

On days 3 and 5, a subset of mice was killed by isoflurane overdose and tissue samples were collected for histopathology and viral titer analyses. The left lung of each mouse was fixed by formalin for sectioning and H&E staining. The superior and middle lobes of the lungs were weighed, homogenized and lysed in 1 ml TRIzol for RNA isolation. The inferior and post-caval lobes of the lungs were weighed and stored at −80 °C until being homogenized in 2 ml DMEM and titrated by plaque assay. Briefly, supernatants of homogenized tissues were serially diluted in DMEM, 250 µl of diluted samples were added to monolayers of Vero-E6 cells, followed by the overlay of 1% low-melting agarose (prepared in 1× DMEM). Plaques were visualized on day 3 after formalin fixation and staining with 0.2% crystal violet. Triplicated wells were performed for each mouse for a mean value.

For the adenovirus (Adv)-hACE2 mouse model, C57BL/6J (B6) mice were intranasally infected with 2.5×10^8 p.f.u. of human ACE2-expressing adenovirus on day −5 before SARS-CoV-2 viral infection. On day 0, Adv-hACE2-treated B6 mice were intranasally infected with 1×10^4 p.f.u. of SARS-CoV-2 virus (USA-WA1/2020) in 30 µl serum-free DMEM. Orlistat (8 mg kg^{-1} body weight) or DMSO/PBS control buffer were administrated daily via intraperitoneal injection. Mice were killed on day 3 for tissue collection.

Screening of shRNA library against SARS-CoV-2. HEK293T-hACE2 cells were plated in 96-well plates (4×10^4 cells per well) and transfected with the shRNA vectors for metabolism genes (150 ng per well). At 72 h post-transfection, cells were subjected to SARS-CoV-2-mNG infection at an MOI of 0.01. Cells were subjected to fluorescence density analyses using FilterMax F5 microplate reader at 48 hpi. The *z* score was calculated with the average and s.d. of each plate. The screening was repeated in two independent experiments for analysis.

Generation of *FASN* KO cells. HEK293T-hACE2 and Caco-2 cells were transduced with Lenti-Cas9 (Lenti-Cas9-Blast, Addgene 52962) and selected with blasticidin (10 mg ml^{-1}) for 14 d. The expression of Cas9 was validated by western blotting. The HEK293T-hACE2-Cas9 cells were then transduced with *FASN* sgRNA lentivirus and selected with puromycin (1 mg ml^{-1}) for 7 d. The *FASN* KO bulk cells were plated into 96-well plates (0.3 cells per well) for *FASN* KO single-cell clone generation. The sequences of *FASN* sgRNA are as follows: 5′-TTCTGGGACAACCTCATCGG-3′, 5′-TCCATCGTGTGTGCCTGCTT-3′.

Plaque assay. Vero-E6 cells were plated as confluent monolayers in 12-well tissue culture plates. Medium was removed and wells was washed with DMEM without FBS. Then, 250 µl of serially diluted cell culture supernatant or homogenized tissue lysates was added into the wells, followed by an incubation of 45 min in 37 °C, 5% CO_2 incubator with a gentle shake. After viral adsorption, supernatant was removed from the well and cells were overlaid with the overlay medium (1:1 mixture of 2% low-melting agarose solution with 2× DMEM). Three days post-infection, cells were fixed with 4% formaldehyde for 24 h. Agar plugs were then removed and cells were stained with 0.2% crystal violet to count plaques for the calculation of viral titers.

Fluorescence assay and quantification of SARS-CoV-2 infection. SARS-CoV-2-mNG virus (icSARS-CoV-2-mNG)-infected HEK293T-hACE2, Caco-2 or MEF-hACE2 cells were subjected to fluorescence-based imaging assay at 24 h after infection or indicated time point. Live cell nucleic acid fluorescent dye Hoechst 33342 was added to the infected cell medium at a final concentration of 1 µg ml^{-1} and was incubated at 37 °C, 5% CO_2 for at least 30 min before imaging. Images of green fluorescence (FITC channel) and Hoechst 33342 (DAPI channel) were acquired using Revolve Fluorescence Microscope (ECHO). The fluorescence intensity of images was analyzed by ImageJ v.1.53e. Green fluorescence intensity was normalized by Hoechst 33342 fluorescence intensity of the same image. The relative infection was determined by the normalized green fluorescence intensity and compared with the control cells (DMSO-treated or other control group indicated elsewhere).

Inhibitor and palmitic acid treatments. One day before treatment, HEK293T-hACE2 (1×10^5 cells per well), Caco-2 (2×10^5 cells per well) or MEF-hACE2 cells (5×10^4 cells per well) were seeded in 24-well plates in culture medium and incubated at 37 °C, 5% CO_2 cell culture incubator. Indicated concentration of FAS inhibitors was added to the cell culture medium at 16 h before infection and maintained in the medium during infection. Pre-treated cells were infected with the SARS-CoV-2 virus or other strains as indicated at an MOI of 0.01 (HEK293T-hACE2 and MEF-hACE2) or 0.05 (Caco-2). Viral RNA or supernatant samples were collected as described in the SARS-CoV-2 viral RNA isolation and quantitative analysis and plaque assay sections in Methods.

For inhibitor dose titration, we generated a fourfold serial dilution of selected eight inhibitors with different starting concentrations of 20 µM (orlistat, FASN-IN-4, FT113), 320 nM (TVB-2640, TVB-3166, GSK-214069) or 80 nM

(TVB-3664, remdesivir). Diluted inhibitors were added to the cells 16 h before infection and maintained in the medium during infection. After being transferred to the BSL3 facility, pre-treated cells were infected with the SARS-CoV-2-mNG virus (icSARS-CoV-2-mNG) with an MOI of 0.01. Fluorescence assay and quantification of SARS-CoV-2 infection were performed at 24 h after infection as described in the fluorescence assay and quantification of SARS-CoV-2 infection section in Methods. A four-parameter logistic nonlinear regression model was used to calculate EC_{50} by GraphPad Prism v.8.0.2 software.

For palmitic acid treatment, BSA-conjugated palmitic acid (PA-BSA; cat. no. P0500, Sigma) was prepared as previously described[48]. In brief, PA-BSA was diluted in prewarmed cell culture medium and mixed in a water sonicator for 5 min before adding to the cells. After 2 h of incubation in a 37 °C cell culture incubator, PA-BSA-treated cells were infected with SARS-CoV-2. Viral RNA was analyzed 24 h after viral infection by qPCR.

Inhibitors were purchased form Selleck Chem: A769662 (S2697); orlistat (S1629); isoniazid (S1937); desoxyrhaponticin (S3300); fatostatin HBr (S8284); TVB-2640 (S9714); C75 (S8915); FT113 (S6666); EGCG (S2250); betulin (S4754); ACSS2 (S8588); kaempferol (S2314); praeruptorin B (S9392); TVB-3664 (S8563); cerulenin (C2389); G28U CM (5446); GSK-2194069 (5303); curcumin (S1848); and remdesivir (S8932). MedChemExpress supplied FASN-IN-2 (HY-112829); FASN-IN-1 (HY-111777); FASN-IN-4 (HY-12648); and TVB-3166 (HY-120394). TOCRIS supplied G28U CM (5446) and GSK-2194069 (5303). Cerulenin was purchased from Sigma (C2389).

Cytotoxicity assay. One day before inhibitor treatment, 2×10^4 HEK293T-hACE2 cells were seeded in 100 µl cell culture medium in 96-well plates. The next day, a series dilution of each inhibitor at indicated concentration was added to the cells (5 µl per well in cell culture medium). DMSO treatment was set up as negative control and baseline. Cell cultures were incubated for 2 d at 37 °C and 5% CO_2 cell culture incubator. After the incubation period, 10 µl of MTT (5 mg ml^{-1}) labeling reagent was added to each well and the microplate was incubated for 4 h in a cell culture incubator. Then, 100 µl of the solubilization solution (10% SDS in 0.01 M HCl) was added into each well. The plate was then allowed to stand overnight in the cell culture incubator. The 590 nm absorbance of samples was detected using a Synergy 2 Multi-Mode Microplate Reader (BioTek) and analyzed by the software Gene 5 (BioTek).

SARS-CoV-2 viral RNA isolation and quantitative analysis. Total RNA was collected from infected cells or mouse tissues at indicated time point using TRIzol reagent (Thermo Fisher Scientific) and removed from the BSL3 facility. RNA was extracted according to manufacturer's instructions. Then, 1 µg of total RNA was used for RT–PCR using the SuperScript IV Reverse Transcriptase (Thermo Fisher Scientific) and random hexamers. Complementary DNA was diluted by 1:10 and 1 µl diluted cDNA was used for qPCR analysis. The qPCR analysis was performed on the Applied Biosystems QuantStudio 6 Flex Real-Time PCR system (Thermo Fisher Scientific) with iTaq Universal SYBR Green Supermix (Bio-Rad). Each sample was run in three or four technical replicated wells. One primer set (SC2-S-F: GCTGGTGCTGCAGCTTATTA; SC2-S-R: AGGGTCAAGTGCACAGTCTA) targeting SARS-CoV-2 virus spike protein was used to measure the relative SARS-CoV-2 viral RNA and normalized to a human GAPDH primer set (hGAPDH-F: GACAGTCAGCCGCATCTTCT; hGAPDH-R: GCCCAATACGACCAAATCCGT) for human samples and a mouse GAPDH primer set (mGapdh-F: GAAGGGCTCATGACCACAGT; mGapdh-R: GGATGCAGGGATGATGTTCT) for mouse samples. An in-house constructed spike protein expression plasmid was used to generate the standard curve of absolute quantification PCR analysis. The results were analyzed using software QuantStudio Software v.1.3 (Thermo Fisher Scientific). Each assay was performed in triplicate with four technical replicates and each assay included no-template negative controls.

Time-of-addition assay. A number of 1×10^5 HEK293T-hACE2 cells were seeded in 24-well plates in culture medium (DMEM + 10% FBS + 1× penicillin-streptomycin) and incubated for 24 h at 37 °C, 5% CO_2 cell culture incubator. Inhibitors were added to the medium at indicated time point (−16 h, −1 h, 0 h, 1 h, 2 h, 4 h and 6 h), then the cells were transferred into the BSL3 facility before infection. SARS-CoV-2 virus was added to medium at an MOI of 0.01 at the time point of hour 0. Before sample collection, cells were washed twice in PBS. To determine the SARS-CoV-2 virus inhibition ability, total RNA of infected cells was collected 24 h after infection by TRIzol reagent (Thermo Fisher Scientific) according to manufacturer's instructions and analyzed by qPCR as previously described in the SARS-CoV-2 viral RNA isolation and quantitative analysis section in Methods.

Virus replication assay. A total of 1×10^5 HEK293T-hACE2 cells were seeded in 24-well plates in culture medium (DMEM, 10% FBS, 1× penicillin-streptomycin) and incubated for 24 h at 37 °C, 5% CO_2 cell culture incubator. Inhibitors were added to the medium 1 d before infection (−16 h). Pre-treated cells were transferred into the BSL3 facility and washed twice with DMEM without FBS. SARS-CoV-2 virus was diluted into 200 µl of DMEM without FBS at an MOI of 0.01 and added to the washed cells. Cells with infectious medium were incubated on a rocker for 45 min at 37 °C, 5% CO_2. After infection, infectious medium was removed and washed twice in PBS. Fresh cell culture medium (DMEM, 10% FBS, 1× penicillin-streptomycin) containing inhibitors at indicated concentrations was added to infected cells and incubated at 37 °C, 5% CO_2. Samples were collected at the indicated time points after infection (0 h, 4 h, 8 h, 16 h, 24 h, 32 h, 48 h and 72 h). To determine viral RNA amplification, RNA samples of infected cells were collected using TRIzol reagent (Thermo Fisher Scientific) according to manufacturer's instructions and analyzed by qPCR as described in the SARS-CoV-2 viral RNA isolation and quantitative analysis section in Methods. To determine viral particle generation, supernatant was collected at the indicated time points. Cells or debris were removed by centrifugation at 500*g* for 3 min. A plaque assay was performed to detect the infectious particle number as described in the plaque assay section in Methods.

Protein expression analysis. Whole-cell extracts of cultured cells were isolated in with lysis and extraction buffer (50 mM HEPES, 150 mM NaCl, 1 mM EDTA, 10% glycerol, 1.5 mM $MgCl_2$ and 1% Triton X-100). Cell debris was removed by centrifugation for 20 min at 12,000*g* at 4 °C in a microcentrifuge. Lysate was mixed with 5× SDS loading buffer and heated for 5 min at 100 °C. Prepared samples were resolved by 10% SDS–PAGE and transferred to PVDF membranes (Bio-Rad). The membrane was blocked for 1 h at room temperature using blocking buffer (5% nonfat dried milk diluted in TBST). Blots were incubated with anti-FAS monoclonal antibody (3180S, clone C20G5, Cell Signaling Technology) diluted at 1:1,000. Protein expression was normalized to β-actin (sc-47778, clone C4, Santa Cruz Biotechnology) diluted at 1:2,000. The HRP-conjugated anti-mouse IgG antibody (31430, clone 31430, Thermo Fisher Scientific) and the HRP-conjugated anti-rabbit IgG antibody (32460, clone 32460, Thermo Fisher Scientific) were used to detect primary antibodies at 1:10,000 dilution. HRP was detected using chemiluminescent HRP substrate (Millipore). Digital images were acquired with the ChemiDoc XRS+ System and analyzed by Image Lab v.5.1 (Bio-Rad).

Free fatty acid assay. The free fatty acid assay was performed with the Free Fatty Acid Assay kit (cat. no. Ab65341, Abcam) according to the manufacturer's instructions with some modifications. Briefly, SARS-CoV-2 virus-infected and non-infected cells were washed with PBS and fixed with 1% SDS solution for 1 h. Collected cell lysates were homogenized in chloroform and incubated on ice for 30 min. The organic phase was collected after centrifuge and vacuumed dry to remove trace chloroform. Dried lipids were dissolved in Fatty Acid Assay Buffer for further assay procedures. Measurement was performed on a microplate reader at Ex/Em = 535/587 nm for fluorometric assay immediately after the reaction was completed.

Palmitoylated protein assay. The palmitoylated protein assay was performed with the EZClick Palmitoylated Protein Assay kit-Red (cat. no. K416, BioVision) according to the manufacturer's instructions. Briefly, cells were seeded in 96-well plates and treated with FAS inhibitors for 24 h before the assay. Next day, cell medium was changed with fresh medium containing inhibitors and 1× EZClick Palmitic Acid Label probe for another 24 h. After incubation, cells were fixed, permeabilized, stained with 1× EZClick Reaction Cocktail and DAPI and evaluated by fluorescence microscope imaging (ZOE Fluorescent Cell Imager).

Histology and microscopy. Fresh lung tissues were fixed with 10% formalin for 24 h and then sent to USC School of Pharmacy Histology Laboratory for further processing and H&E staining. Slides were evaluated by a pathologist under a microscope and fields were randomly selected for analysis. Pictures were taken at ×4 and ×10 magnification using the Olympus BX61 microscope along with DP71 digital camera (Olympus).

Histopathology score in SARS-CoV-2 model. After H&E staining, the size of pulmonary lesions was determined by the mean percentage of affected area in each section of lobes from each animal. Lung tissues were then scored on a 0–4 system for pathological severity in these infected mice: 0, no pathological change; 1, affected area (≤10%); 2, affected area (≤30% and >10%); 3, affected area (≤60% and >30%); and 4, affected area (>60%).

Statistical analysis. Descriptive statistics, including means, s.d., medians and ranges, were computed for each group. Data are represented as mean ± s.d. unless otherwise indicated. The sample size for each experiment is included in the figure legends. Statistical analyses were performed with unpaired Student's *t*-test, one-way ANOVA followed by Dunnett's post-test, two-way ANOVA followed by Tukey post-test and two-way ANOVA followed by Sidak's post-test, as indicated in figure legends. Differences in animal survival were evaluated with Mantel–Cox log-rank test. $^*P < 0.05$, $^{**}P < 0.01$, $^{***}P < 0.001$ and $^{****}P < 0.0001$ versus control groups. NS denotes not significant (P value >0.05). All analyses were performed with GraphPad Prism v.8.0.2 (GraphPad Software).

Reporting Summary. Further information on research design is available in the Nature Research Reporting Summary linked to this article.

Data availability

shRNA screening data are provided in Supplementary Table 1. Uncropped western blot images and statistical source data are provided with this paper. Further supporting data are available from the corresponding author R.-F.W. (rongfuwa@usc.edu) upon reasonable request. Source data are provided with this paper.

Received: 21 May 2021; Accepted: 14 September 2021;
Published online: 27 September 2021

References

1. Peiris, J. S. et al. Coronavirus as a possible cause of severe acute respiratory syndrome. *Lancet* **361**, 1319–1325 (2003).
2. Zaki, A. M., van Boheemen, S., Bestebroer, T. M., Osterhaus, A. D. & Fouchier, R. A. Isolation of a novel coronavirus from a man with pneumonia in Saudi Arabia. *N. Engl. J. Med.* **367**, 1814–1820 (2012).
3. de Wit, E., van Doremalen, N., Falzarano, D. & Munster, V. J. SARS and MERS: recent insights into emerging coronaviruses. *Nat. Rev. Microbiol.* **14**, 523–534 (2016).
4. Wadman, M. Why obesity worsens COVID-19. *Science* **369**, 1280–1281 (2020).
5. Stefan, N., Birkenfeld, A. L. & Schulze, M. B. Global pandemics interconnected - obesity, impaired metabolic health and COVID-19. *Nat. Rev. Endocrinol.* **17**, 135–149 (2021).
6. Simonnet, A. et al. High prevalence of obesity in severe acute respiratory syndrome coronavirus-2 (SARS-CoV-2) requiring invasive mechanical ventilation. *Obesity* **28**, 1195–1199 (2020).
7. Drucker, D. J. Diabetes, obesity, metabolism, and SARS-CoV-2 infection: the end of the beginning. *Cell Metab.* **33**, 479–498 (2021).
8. Williamson, E. J. et al. Factors associated with COVID-19-related death using OpenSAFELY. *Nature* **584**, 430–436 (2020).
9. Jin, Z. et al. Structure of M(pro) from SARS-CoV-2 and discovery of its inhibitors. *Nature* **582**, 289–293 (2020).
10. Zhang, L. et al. Crystal structure of SARS-CoV-2 main protease provides a basis for design of improved α-ketoamide inhibitors. *Science* **368**, 409–412 (2020).
11. Li, Z. et al. Identify potent SARS-CoV-2 main protease inhibitors via accelerated free energy perturbation-based virtual screening of existing drugs. *Proc. Natl Acad. Sci. USA* **117**, 27381–27387 (2020).
12. Qiao, J. et al. SARS-CoV-2 M(pro) inhibitors with antiviral activity in a transgenic mouse model. *Science* https://doi.org/10.1126/science.abf1611 (2021).
13. Riva, L. et al. Discovery of SARS-CoV-2 antiviral drugs through large-scale compound repurposing. *Nature* **586**, 113–119 (2020).
14. Yang, L. et al. Identification of SARS-CoV-2 entry inhibitors among already approved drugs. *Acta Pharmacol. Sin.* https://doi.org/10.1038/s41401-020-00556-6 (2020).
15. Yuan, S. et al. Clofazimine broadly inhibits coronaviruses including SARS-CoV-2. *Nature* https://doi.org/10.1038/s41586-021-03431-4 (2021).
16. Beigel, J. H. et al. Remdesivir for the treatment of COVID-19: final report. *N. Engl. J. Med.* **383**, 1813–1826 (2020).
17. Wang, Y. et al. Remdesivir in adults with severe COVID-19: a randomised, double-blind, placebo-controlled, multicentre trial. *Lancet* **395**, 1569–1578 (2020).
18. Goldman, J. D. et al. Remdesivir for 5 or 10 days in patients with severe COVID-19. *N. Engl. J. Med.* **383**, 1827–1837 (2020).
19. Hoffmann, H. H. et al. TMEM41B is a pan-flavivirus host factor. *Cell* **184**, 133–148 (2021).
20. Schneider, W. M. et al. Genome-scale Identification of SARS-CoV-2 and pan-coronavirus host factor networks. *Cell* **184**, 120–132 (2021).
21. Wei, J. et al. Genome-wide CRISPR screens reveal host factors critical for SARS-CoV-2 infection. *Cell* **184**, 76–91 (2021).
22. Wang, R. et al. Genetic screens identify host factors for SARS-CoV-2 and common cold coronaviruses. *Cell* **184**, 106–119 (2021).
23. Daniloski, Z. et al. Identification of required host factors for SARS-CoV-2 infection in human cells. *Cell* **184**, 92–105 (2021).
24. Wong, J. P. & Damania, B. SARS-CoV-2 dependence on host pathways. *Science* **371**, 884–885 (2021).
25. White, K. M. et al. Plitidepsin has potent preclinical efficacy against SARS-CoV-2 by targeting the host protein eEF1A. *Science* **371**, 926–931 (2021).
26. Ho, J. S. Y. et al. TOP1 inhibition therapy protects against SARS-CoV-2-induced lethal inflammation. *Cell* **184**, 2618–2632 (2021).
27. Soliman, S., Faris, M. E., Ratemi, Z. & Halwani, R. Switching host metabolism as an approach to dampen SARS-CoV-2 infection. *Ann. Nutr. Metab.* **76**, 297–303 (2020).
28. Tanner, J. E. & Alfieri, C. The fatty acid lipid metabolism nexus in COVID-19. *Viruses* https://doi.org/10.3390/v13010090 (2021).
29. Ayres, J. S. A metabolic handbook for the COVID-19 pandemic. *Nat. Metab.* **2**, 572–585 (2020).
30. Mullen, P. J. et al. SARS-CoV-2 infection rewires host cell metabolism and is potentially susceptible to mTORC1 inhibition. *Nat. Commun.* **12**, 1876 (2021).
31. Zhang, Y. et al. SARS-CoV-2 hijacks folate and one-carbon metabolism for viral replication. *Nat. Commun.* **12**, 1676 (2021).
32. Xie, X. et al. An infectious cDNA clone of SARS-CoV-2. *Cell Host Microbe* **27**, 841–848 (2020).
33. Kridel, S. J., Axelrod, F., Rozenkrantz, N. & Smith, J. W. Orlistat is a novel inhibitor of fatty acid synthase with antitumor activity. *Cancer Res.* **64**, 2070–2075 (2004).
34. Wu, Z. et al. Palmitoylation of SARS-CoV-2 S protein is essential for viral infectivity. *Signal Transduct. Target Ther.* **6**, 231 (2021).
35. Winkler, E. S. et al. SARS-CoV-2 infection of human ACE2-transgenic mice causes severe lung inflammation and impaired function. *Nat. Immunol.* **21**, 1327–1335 (2020).
36. Rathnasinghe, R. et al. Comparison of transgenic and adenovirus hACE2 mouse models for SARS-CoV-2 infection. *Emerg. microbes Infect.* **9**, 2433–2445 (2020).
37. Davies, N. G. et al. Estimated transmissibility and impact of SARS-CoV-2 lineage B.1.1.7 in England. *Science* https://doi.org/10.1126/science.abg3055 (2021).
38. Davies, N. G. et al. Increased mortality in community-tested cases of SARS-CoV-2 lineage B.1.1.7. *Nature* https://doi.org/10.1038/s41586-021-03426-1 (2021).
39. Washington, N. L. et al. Emergence and rapid transmission of SARS-CoV-2 B.1.1.7 in the United States. *Cell* **184**, 2587–2594 (2021).
40. Zhou, D. et al. Evidence of escape of SARS-CoV-2 variant B.1.351 from natural and vaccine-induced sera. *Cell* https://doi.org/10.1016/j.cell.2021.02.037 (2021).
41. Planas, D. et al. Sensitivity of infectious SARS-CoV-2 B.1.1.7 and B.1.351 variants to neutralizing antibodies. *Nat. Med.* https://doi.org/10.1038/s41591-021-01318-5 (2021).
42. Lopez Bernal, J. et al. Effectiveness of COVID-19 vaccines against the B.1.617.2 (δ) variant. *N. Engl. J. Med.* **385**, 585–594 (2021).
43. Sheikh, A. et al. SARS-CoV-2 δ VOC in Scotland: demographics, risk of hospital admission, and vaccine effectiveness. *Lancet* **397**, 2461–2462 (2021).
44. Lorizate, M. & Krausslich, H. G. Role of lipids in virus replication. *Cold Spring Harb. Perspect. Biol.* **3**, a004820 (2011).
45. Heck, A. M., Yanovski, J. A. & Calis, K. A. Orlistat, a new lipase inhibitor for the management of obesity. *Pharmacotherapy* **20**, 270–279 (2000).
46. Hitakarun, A. et al. Evaluation of the antiviral activity of orlistat (tetrahydrolipstatin) against dengue virus, Japanese encephalitis virus, Zika virus and chikungunya virus. *Sci. Rep.* **10**, 1499 (2020).
47. Williams, C. F. et al. Inhibitors of VPS34 and fatty-acid metabolism suppress SARS-CoV-2 replication. *Cell Reports* **36**, 109479 (2021).
48. Kim, J. Y. et al. Palmitic acid-BSA enhances amyloid-β production through GPR40-mediated dual pathways in neuronal cells: involvement of the Akt/mTOR/HIF-1α and Akt/NF-κB pathways. *Sci. Rep.* **7**, 4335 (2017).

Acknowledgements

We thank P.Y. Shi from the University of Texas Medical Branch for the generous gift of the SARS-CoV-2-mNG virus; W. Wang (MD Anderson Cancer Center) for histopathological scoring; C. Qin and Y. Rao from USC Herman Ostrow School of Dentistry for technical supports; L. Comai and J. Marshall from the USC BSL3 Core for supports and resources; K. O'Brien from the USC Environmental Health & Safety for biosafety supports; J. Watanabe and Z. Zhang from the Histology Core in USC School of Pharmacy for mouse tissue processing and S. Richman for critical reading and editing of our manuscript. This work was, in part, supported by USC Startup Fund and grants from the National Cancer Institute, National Institutes of Health (R01CA101795, R01CA246547 and U54CA210181) and Department of Defense CDMRP BCRP (BC151081) and LCRP (LC200368) to R.F.W.

Author contributions

R.-F.W. supervised the entire study. R.-F.W., J.C., C.X. and Y.D. designed the experiments. J.C. and C.X. performed in vitro BSL3 experiments with SARS-CoV-2 virus and variants including viral infection, sample collection and analysis. C.X. and J.C. performed in vivo ABSL3 experiments with SARS-CoV-2 virus-infected mice, including infection, drug administration, necropsies and tissue analysis. Y.D. performed plasmid preparation, transfection, knockout cell construction and western blotting. J.C. constructed the screening shRNA library and performed fluorescence imaging. Y.D., S.L., P.Z. and C.C. performed animal breeding and genotyping. J.H. requested the SARS-CoV-2 viruses and performed initial expansion. T.D., X.L., B.Y. and C.Q. provided assistance with some experiments. J.C., C.X., Y.D. and H.Y.W. performed data analyses. C.X., J.C., Y.D. and R.-F.W. wrote the paper.

Competing interests
The authors declare no competing interests.

Additional information
Extended data is available for this paper at https://doi.org/10.1038/s42255-021-00479-4.

Supplementary information The online version contains supplementary material available at https://doi.org/10.1038/s42255-021-00479-4.

Correspondence and requests for materials should be addressed to Rong-Fu Wang.

Peer review information *Nature Metabolism* thanks the anonymous reviewers for their contribution to the peer review of this work. Primary handling editor: Christoph Schmitt.

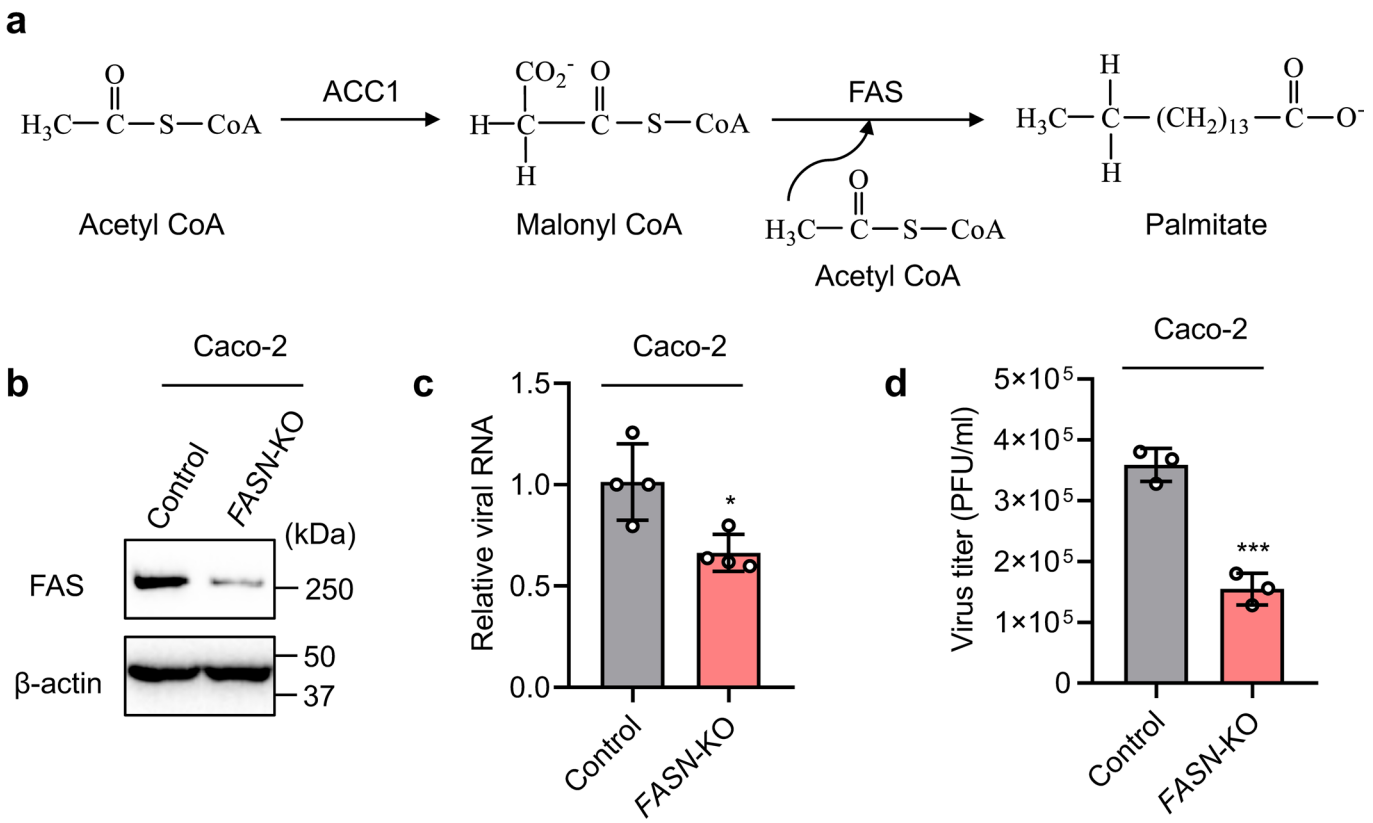

Extended Data Fig. 1 | FAS deficiency inhibits SARS-CoV-2 infection. (**a**) The functional role of ACC1 and FAS in the fatty acid synthesis process. (**b**) Representative western blot result for FAS expression in Caco-2 cells transduced with puro-guide control or FASN sgRNA lentivirus. (**c**) FASN KO inhibits SARS-CoV-2 viral replication. Control and FAS-deficient Caco-2 cells were infected with SARS-CoV-2 with an MOI of 0.05. Viral RNA in the infected cells by qPCR analysis at 24 hpi (**c**). Virus titer in the supernatant by plaque assay at 3 dpi (**d**). Data in **c** and **d** are representative of three independent experiments and are plotted as the mean ± SD (n = 4 (**d**), n = 4 (**c**) per group). The experiment in b has been independently repeated three times with similar result. Statistical analysis was performed using two-side unpaired Student's t-test. *$p < 0.05$, ***$p < 0.001$.

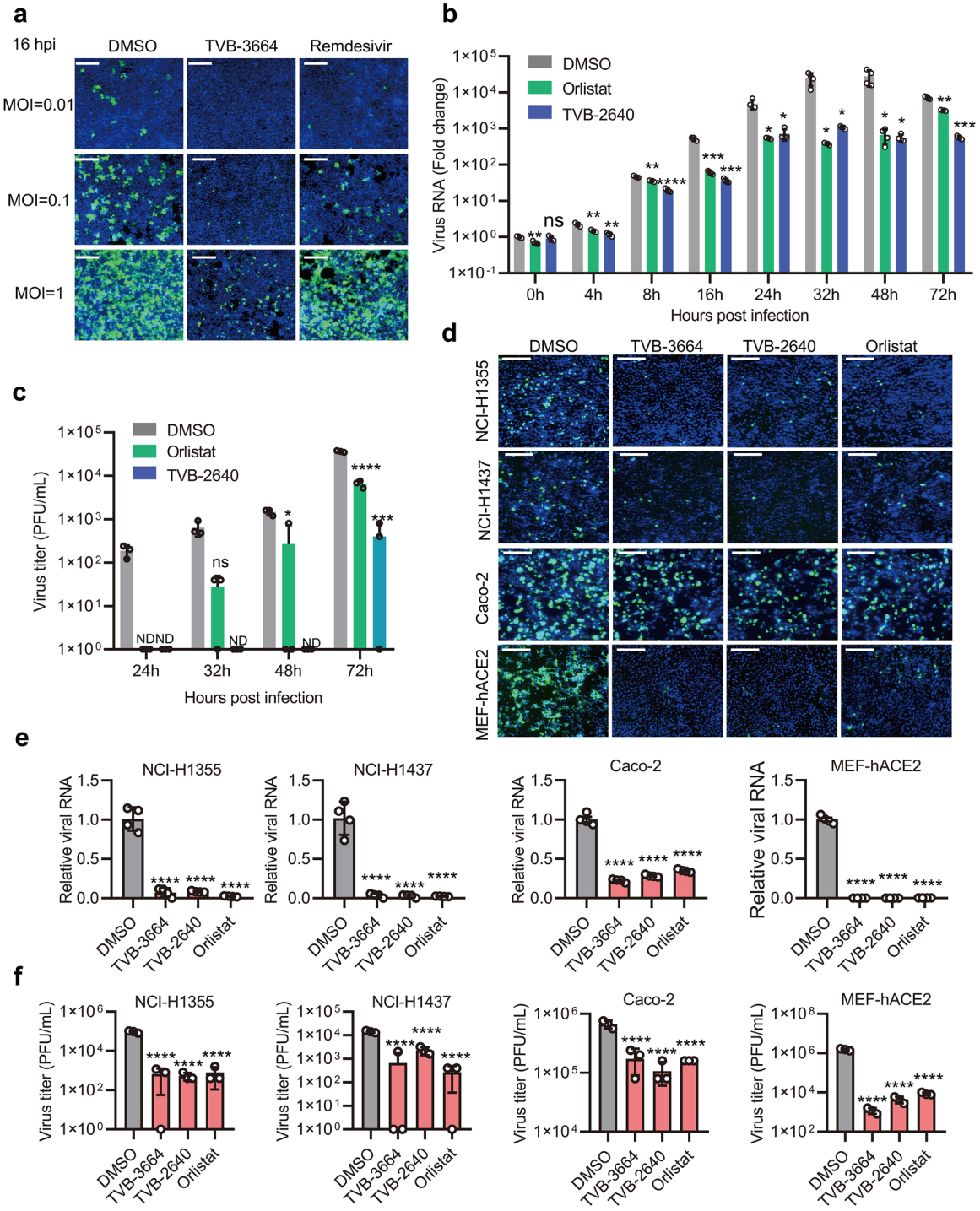

Extended Data Fig. 2 | See next page for caption.

Extended Data Fig. 2 | Fatty acid synthase inhibitors suppress SARS-CoV-2 virus replication. (**a**) Representative fluorescence images for data in Fig. 2c. Scale bar: 200 μm. (**b-c**) FAS inhibitors repress SARS-CoV-2 viral replication. HEK293T-hACE2 cells treated with Orlistat (1 μM) or TVB-2640 (100 nM) and infected with SARS-CoV-2 at h 0. (**b**) Viral RNA by qPCR at indicated time points. (**c**) Infectious viral titers in supernatant by plaque assay. (**d**) Representative fluorescence images of SARS-CoV-2-mNG infected multiple cell lines. Indicated cells were pre-treated with FAS inhibitors at the following concentration: NCI-H1355 and NCI-1437 (Orlistat 20 μM, TVB-2640 2 μM and TVB-3664 1 μM); Caco-2 (Orlistat 80 μM, TVB-2640 2 μM and TVB-3664 1 μM); MEF-hACE2 (Orlistat 5 μM, TVB-2640 1 μM and TVB-3664 0.5 μM), from 16 h before infection and then infected with SARS-CoV-2-mNG at an MOI = 0.1(NCI-H1355, NCI-1437), MOI = 0.05 (Caco-2), MOI = 0.01 (MEF-hACE2). Fluorescence images were acquired at 48 hpi. Hoechst 33342 was used for nuclear staining. Scale bar: 200 μm. (**e**,**f**) Assessment of anti-SARS-CoV-2 ability of FAS inhibitors in multiple cell lines. Indicated cells were pre-treated with FAS inhibitors and infected with SARS-CoV-2 as described in Extended Data Fig. 2d. 24 h after infection, cells were collected for quantification of intracellular viral RNA by qPCR (**e**), supernatants were collected for quantification of viral titer by plaque assay (**f**). Data in b-c and e-f are representative of three independent experiments and are plotted as the mean ± SD (n = 3 (c, f), n = 4 (**b**, **e**) per group). The experiment in **a** and **d** have been independently repeated three times with similar result. ND: not detected. Statistical analyses were performed with two-way ANOVA followed by Dunnett's post-test (**b**, **c**) and one-way ANOVA followed by Dunnett's post-test (**e**,**f**). *$p < 0.05$, **$p < 0.01$, ***$p < 0.001$ and ****$p < 0.0001$, ns, not significant ($p > 0.05$), comparing to DMSO-treated cells (**e**, **f**) or DMSO-treated cells at each time point (**b**, **c**).

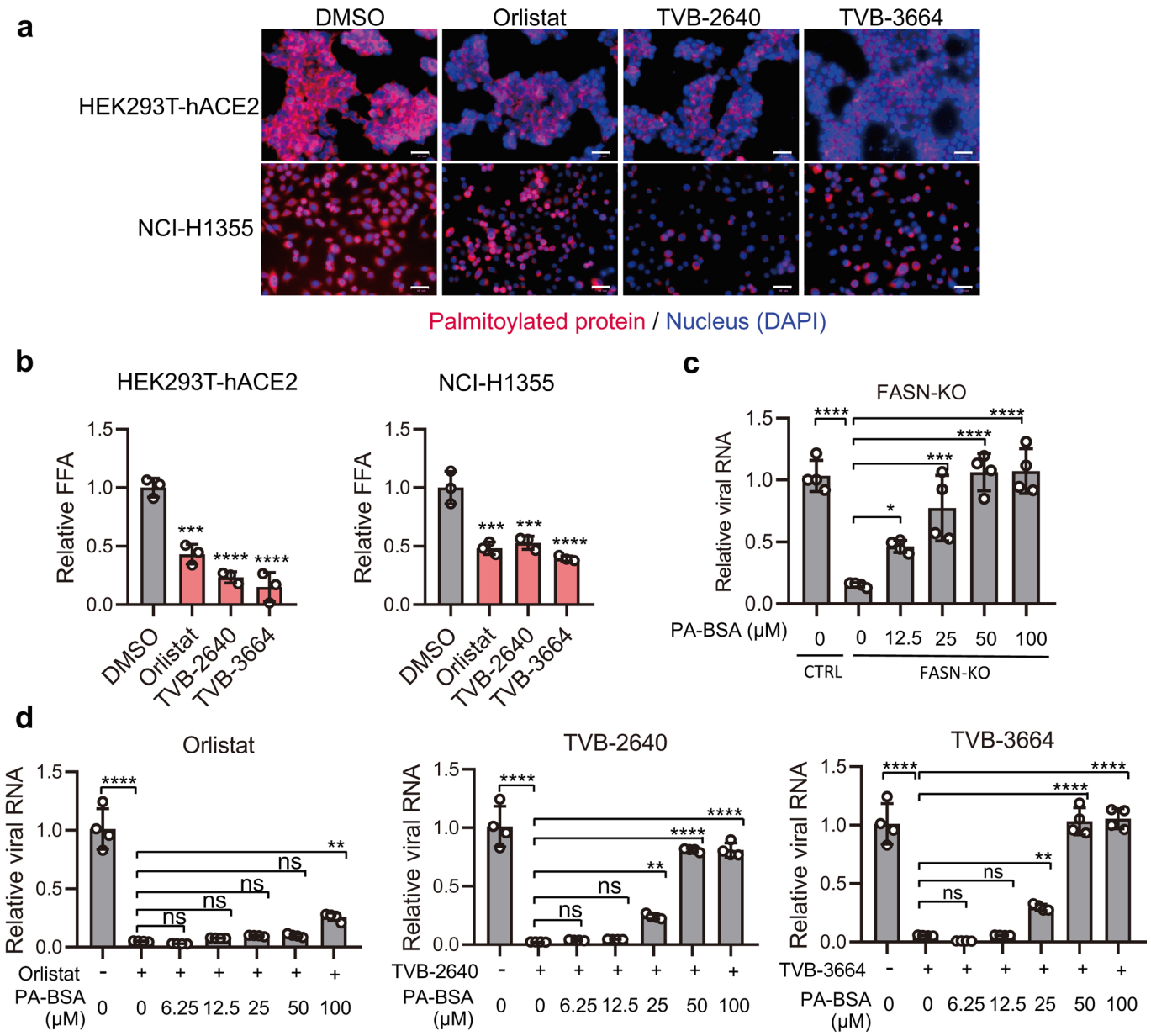

Extended Data Fig. 3 | Palmitic acid reverses the effects of knockout and inhibition of fatty acid synthase on viral replication. (**a**) Representative fluorescence images of palmitoylated protein assay. HEK293T-hACE2 and NCI-H1355 cells were treated with FAS inhibitors (HEK293T-hACE2 cells: Orlistat 1 μM, TVB-2640 100 nM, and TVB-3664 20 nM; NCI-H1355 cells: Orlistat 20 μM, TVB-2640 2 μM, and TVB-3664 1 μM) for 24 h and the EZClick™ palmitic acid label was added to the medium for another 24 h. Cells were then processed and analyzed by microscopy following the manufacturer's instruction. Scale bar: 40 μm. (**b**) HEK293T-hACE2 and NCI-H1355 cells were treated with FAS inhibitors (HEK293T-hACE2 cells: Orlistat 1 μM, TVB-2640 100 nM, and TVB-3664 20 nM; NCI-H1355 cells: Orlistat 20 μM, TVB-2640 2 μM, and TVB-3664 1 μM) for 24 h, then analyzed with FFA assay following the manufacturer's instruction. (**c**) Palmitic acid reverses the effects of fatty acid synthase knockout on viral replication. FASN knockout HEK293T-hACE2 cells were pre-treated with bovine serum albumin- conjugated palmitic acid (PA-BSA) at indicated final concentrations 2 hours before infection. The cells were infected with the SARS-CoV-2 virus at an MOI of 0.01. Viral RNA was analyzed at 24 hpi by qPCR. Wild-type (WT) HEK293T-hACE2 were used as a negative control. (**d**) Palmitic acid reverses the effects of FAS inhibitors on viral replication. HEK293T-hACE2 cells were pre-treated FAS inhibitors (Orlistat 1 μM, TVB-2640 100 nM, and TVB-3664 20 nM) for 14 h. PA-BSA was then added at the indicated final concentrations and the cells were treated for another 2 h. The cells were infected with SARS-CoV-2 virus at an MOI of 0.01. Viral RNA was analyzed at 24 hpi by qPCR. DMSO treated cells were used as a negative control. Data in **b**-**d** are representative of three independent experiments and are plotted as the mean ± SD (n = 3 (**b**), n = 4 (**c**, **d**) per group). The experiment in **a** has been independently repeated three times with similar result. One-way ANOVA followed by Dunnett's post-test was used for statistical analysis (**b-d**). *p < 0.05, **p < 0.01, ****p < 0.0001, and ns, not significant (p > 0.05), comparing to BSA-treated FASN-KO HEK293T-hACE2 cells (**c**), or DMSO- (**b**) / BSA- (**d**) treated HEK293T-hACE2 cells.

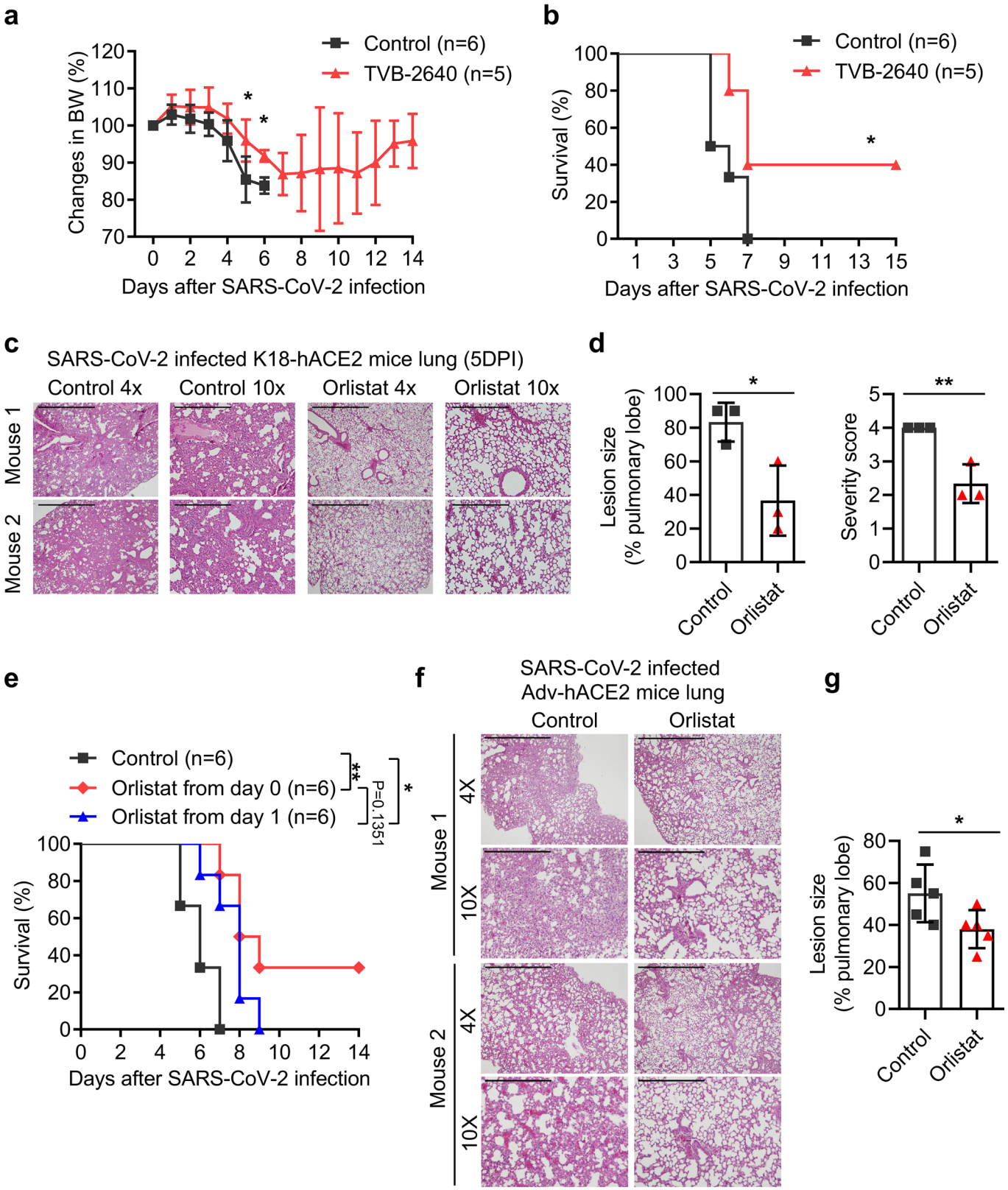

Extended Data Fig. 4 | See next page for caption.

Extended Data Fig. 4 | FAS inhibitors inhibit SARS-CoV-2 infection in vivo and prolong mouse survival. (**a**,**b**) TVB-2640 reduces body weight loss and prolongs mouse survival after SARS-CoV-2 infection. K18-hACE2 transgenic mice were infected with SARS-CoV-2 virus (intranasal infection, 1×104 PFU/mouse, USA-WA1/2020) and i.p. injected with TVB-2640 (8 mg/kg body weight) daily from day 0 to day 5. Body weight changes (**a**) and survival curves (**b**) were observed and analyzed. (**c**,**d**) Orlistat reduces disease progression in lung tissues after SARS-CoV-2 infection. K18-hACE2 transgenic mice were similarly infected with SARS-CoV-2 and i.p. injected with Orlistat as in Fig. 3. (**c**) Histopathology of formalin-fixed and H&E-stained lung tissues on day 5. (**d**) Analyses of pulmonary lesion sizes and pathological severity scores, based on the percentage of affected area in lung tissues. Scale bar: 400 μm for 10X and 1 mm for 4X. (**e**) Orlistat treatment provides therapeutic effects after SAR-CoV-2 infection. K18-hACE2 transgenic mice were similarly infected with SARS-CoV-2 as in Fig. 3, and intraperitoneally (i.p.) injected with Orlistat (8 mg/kg body weight) daily from day 0 or 1 to day 5. Survival curves were observed and analyzed. (**f**,**g**) Orlistat reduces disease progression in adenovirus-hACE2 model. WT B6 mice were intranasally infected with adenovirus (Adv)-hACE2 to induce the ACE2 expression in lung epithelial cells. After 5 days, mice were similarly infected with SARS-CoV-2 and i.p. injected with Orlistat as in Fig. 3. (**f**) Histopathology of formalin-fixed and H&E-stained lung tissues on day 3. (**g**) Analyses of pulmonary lesion sizes. Scale bar: 400 μm for 10X and 1 mm for 4X. Panels **a**, **b**, and **e** are combined data of two independent experiments and are plotted as the mean ± SD, d and g are representative data plotted as the mean ± SD of 3 mice (**d**) or 5 mice (**g**). Statistical differences between groups were calculated using two-way ANOVA followed by Sidak's post-test (**a**), two-side unpaired Student's t test (**d** and **g**), and Mantel-Cox log-rank test (**b** and **e**). *$p < 0.05$; **$p < 0.01$.

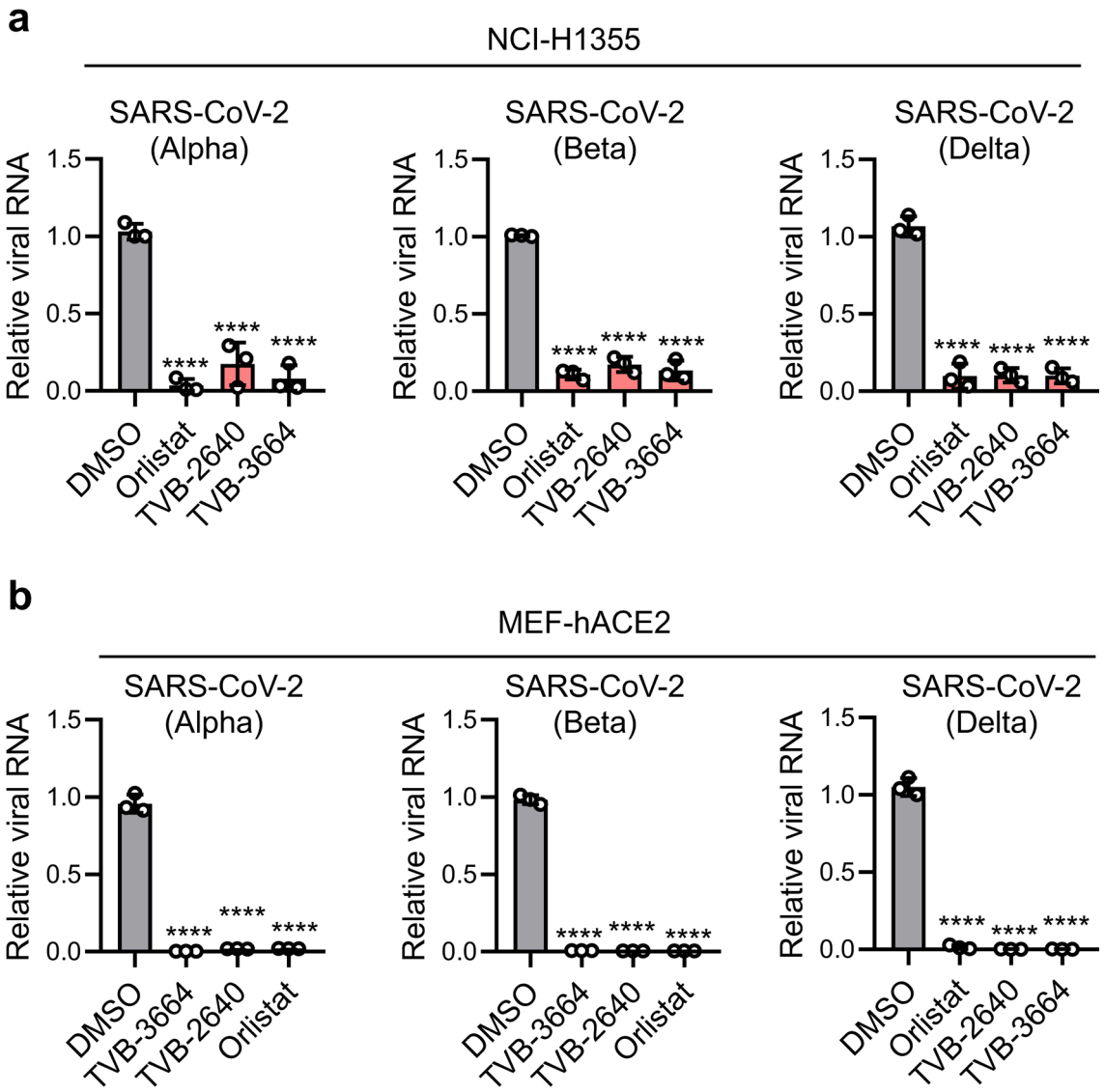

Extended Data Fig. 5 | Fatty acid synthase inhibitors suppress the replication of SARS-CoV-2 variants. (**a**) NCI-H1355 cells were pre-treated with FAS inhibitors, Orlistat (20 μM), TVB-2640 (2 μM), or TVB-3664 (1 μM) for 16 h and infected with SARS-CoV-2 variants with an MOI of 0.1. The cells were analyzed by qPCR for viral RNA at 48 hpi. (**b**) MEF-hACE2 cells were pre-treated with FAS inhibitors, Orlistat (5 μM), TVB-2640 (1 μM), or TVB-3664 (0.5 μM) for 16 h and infected with SARS-CoV-2 variants with an MOI of 0.05. The cells were analyzed by qPCR for viral RNA at 48 hpi. Data in **a-b** are representative of three independent experiments and are plotted as the mean ± SD (n = 3 (**a**, **b**) per group). Statistical analyses were performed using one-way ANOVA followed by Dunnett's post-test. ****$p < 0.0001$.

nature research

Corresponding author(s): Rong-Fu Wang

Last updated by author(s): 9-9-2021

Reporting Summary

Nature Research wishes to improve the reproducibility of the work that we publish. This form provides structure for consistency and transparency in reporting. For further information on Nature Research policies, see our Editorial Policies and the Editorial Policy Checklist.

Statistics

For all statistical analyses, confirm that the following items are present in the figure legend, table legend, main text, or Methods section.

n/a	Confirmed	
☐	☒	The exact sample size (*n*) for each experimental group/condition, given as a discrete number and unit of measurement
☐	☒	A statement on whether measurements were taken from distinct samples or whether the same sample was measured repeatedly
☐	☒	The statistical test(s) used AND whether they are one- or two-sided *Only common tests should be described solely by name; describe more complex techniques in the Methods section.*
☒	☐	A description of all covariates tested
☐	☒	A description of any assumptions or corrections, such as tests of normality and adjustment for multiple comparisons
☐	☒	A full description of the statistical parameters including central tendency (e.g. means) or other basic estimates (e.g. regression coefficient) AND variation (e.g. standard deviation) or associated estimates of uncertainty (e.g. confidence intervals)
☐	☒	For null hypothesis testing, the test statistic (e.g. *F*, *t*, *r*) with confidence intervals, effect sizes, degrees of freedom and *P* value noted *Give P values as exact values whenever suitable.*
☒	☐	For Bayesian analysis, information on the choice of priors and Markov chain Monte Carlo settings
☒	☐	For hierarchical and complex designs, identification of the appropriate level for tests and full reporting of outcomes
☒	☐	Estimates of effect sizes (e.g. Cohen's *d*, Pearson's *r*), indicating how they were calculated

Our web collection on statistics for biologists contains articles on many of the points above.

Software and code

Policy information about availability of computer code

Data collection	Gene 5 (BioTek), QuantStudio Software v1.3 (Thermo Fisher Scientific), Image lab 5.1 (BioRad), Revolve Fluorescence Microscope (ECHO, San Diego, CA), ZOE fluorescent Cell Imager (Bio-Rad), FilterMax F5 microplate reader.
Data analysis	The following softwares were used for the data analysis in this study: GraphPad Prism 8.0.2; Gene 5 (BioTek). QuantStudio Software v1.3 (Thermo Fisher Scientific). Image lab 5.1 (BioRad), Image J 1.53e.

For manuscripts utilizing custom algorithms or software that are central to the research but not yet described in published literature, software must be made available to editors and reviewers. We strongly encourage code deposition in a community repository (e.g. GitHub). See the Nature Research guidelines for submitting code & software for further information.

Data

Policy information about availability of data

All manuscripts must include a data availability statement. This statement should provide the following information, where applicable:

- Accession codes, unique identifiers, or web links for publicly available datasets
- A list of figures that have associated raw data
- A description of any restrictions on data availability

The following data availability statement was added to the manuscript:
All of our data are publicly available. The shRNA screening data is provided in the Supplementary Table 1. All other raw data are provided in this paper as source data, including the uncropped western blots images and statistical source data. Further supporting information is available from the corresponding author Dr. Rong-Fu Wang (rongfuwa@usc.edu) upon reasonable request.

Field-specific reporting

Please select the one below that is the best fit for your research. If you are not sure, read the appropriate sections before making your selection.

☒ Life sciences ☐ Behavioural & social sciences ☐ Ecological, evolutionary & environmental sciences

For a reference copy of the document with all sections, see nature.com/documents/nr-reporting-summary-flat.pdf

Life sciences study design

All studies must disclose on these points even when the disclosure is negative.

Sample size	Sample sizes calculations of animal experiments were performed by using PASS 2002 (NCSS and PASS, Kaysville, UT) for two normally distributed samples. Based on our preliminary study in the same model, the sample size of 5 mice per group was determined for over 80% power to detect a difference between the groups with a significance level (alpha) of 0.05, or confidence interval of 95%, using a two-sided, two-sample t-test.
Data exclusions	No data has been excluded for statistical analysis.
Replication	We confirmed that all attempts to replicate experiments were successful. All the in vitro experiments were performed independently for at least three times, except the shRNA screening experiment that was performed independently for two times. Most of the in vivo experiments were performed independently for at least two times, except the data in Extended Data Figures 4d and 4g due to the limitation on available animals during Covid-19 pandemic. However, for Extended Data Figures 4d and 4g, consistent findings at different time points or models are shown in Figure 3g, partially indicating that they are replicable. The replication information has been included in the manuscript.
Randomization	All the mice were randomly separated into different groups. In all the experiments, males, females, and age-matched mice were used. For cell culture experiments, cells were prepared and randomly distributed into each well of the plates for our experiments.
Blinding	The screening of shRNA sublibrary for their antiviral activity was blinded. The analysis of pulmonary lesion sizes and pathological severity scores was blinded. For other experiments, they were not blinded due to different treatments or experiments performed by the same person.

Reporting for specific materials, systems and methods

We require information from authors about some types of materials, experimental systems and methods used in many studies. Here, indicate whether each material, system or method listed is relevant to your study. If you are not sure if a list item applies to your research, read the appropriate section before selecting a response.

Materials & experimental systems

n/a	Involved in the study
☐	☒ Antibodies
☐	☒ Eukaryotic cell lines
☒	☐ Palaeontology and archaeology
☐	☒ Animals and other organisms
☒	☐ Human research participants
☒	☐ Clinical data
☒	☐ Dual use research of concern

Methods

n/a	Involved in the study
☒	☐ ChIP-seq
☒	☐ Flow cytometry
☒	☐ MRI-based neuroimaging

Antibodies

Antibodies used	The anti-FAS Monoclonal Antibody (#3180S, clone C20G5, Cell Signaling Technology) diluted at 1:1000. Anti-human β-Actin (sc-47778, clone C4, Santa Cruz Biotechnology) diluted at 1:2000. The HRP-conjugated anti-mouse IgG antibody (#31430, clone 31430, Thermo Fisher Scientific) and the HRP-conjugated anti-rabbit IgG antibody (#32460, clone 32460, Thermo Fisher Scientific) were used to detect the primary antibodies at 1:10000.
Validation	All antibodies were purchased from commercial vendors and have been validated by the companies. The antibodies used to detect human FAS protein expression was further validated by FASN gene specific sgRNA transduced knockout cells, compared with wild-type cells.

Eukaryotic cell lines

Policy information about cell lines

Cell line source(s)	HEK293T-hACE2 cells were requested form BEI Resources (Cat#: NR-52511), Vero E6 (ATCC, Cat#: CRL-1586) and Caco-2 (ATCC, Cat#: HTB-37) NCI-H1355 (Cat#: CRL-5865) and NCI-H1437 (Cat#: CRL-5872) were purchased from ATCC, MEF-hACE2

	(mouse embryonic fibroblasts transduced with human ACE2) cells were generated in our lab.
Authentication	Most of the cells were commercially available cells lines . We have validated the ACE2 expression for HEK293T-hACE2 and MEF-hACE2 cells by western blotting. However, we did not perform authentication testing of these cell lines using different techniques. Thus, these commercially available cells lines were not authenticated.
Mycoplasma contamination	We routinely checked the cells for mycoplasma contamination. They were negative for mycoplasma test.
Commonly misidentified lines (See ICLAC register)	No commonly misidentified cell lines were used in this study.

Animals and other organisms

Policy information about studies involving animals; ARRIVE guidelines recommended for reporting animal research

Laboratory animals	K18-hACE2 (Cat#: 034860) transgenic mice and C57BL/6J (Cat#: 000664) mice were purchased from Jackson Laboratory. In all experiments, 8-10 week-old mice were used; and both males and females mice were age-matched. The detailed housing conditions have been included in the manuscript.
Wild animals	No wild animals were used in this study.
Field-collected samples	No field collected samples were used in this study.
Ethics oversight	The Institutional Animal Care and Use Committee (IACUC) of the University of Southern California

Note that full information on the approval of the study protocol must also be provided in the manuscript.